J. Mech. Phys. Solids 179 (2023) 105347

Contents lists available at ScienceDirect

Journal of the Mechanics and Physics of Solids

journal homepage: www.elsevier.com/locate/jmps

A pseudo-hyperelastic model incorporating the rate effects for isotropic rubber-like materials

Afshin Anssari-Benam [a], Mokarram Hossain [b,*]

[a] Cardiovascular Engineering Research Lab (CERL), School of Mechanical and Design Engineering, University of Portsmouth, Anglesea Road, Portsmouth PO1 3DJ, United Kingdom
[b] Zienkiewicz Institute for Modelling, Data and AI, Faculty of Science and Engineering, Swansea University, Swansea SA1 8EN, United Kingdom

ARTICLE INFO

Keywords:
Rate-dependency
Elastomers
Constitutive modelling
Softening
Rate of deformation

ABSTRACT

An alternative modelling framework is proposed for capturing the *rate*-dependency in the loading and unloading (i.e., with softening) deformation behaviour of a wide range of isotropic incompressible elastomers. The proposed framework departs from the existing approaches in the literature which assume an additive contribution of the 'non-equilibrium', or 'viscous', part to the elastic response. Instead, here it is considered that the model parameters of the basic hyperelastic function *evolve* (i.e., vary) with the deformation *rate*. That is, the basic hyperelastic model parameters are considered as functions of *rate*, given the deformation rate as a parameter and *not* a variable, pre-set in experiments. While the nature, and choice, of this functional dependency is empirical, a simple linear relationship is considered in this work between the parameters of a chosen basic hyperelastic model and the applied deformation rate. Using this specialisation, the model is applied to extant experimental data of a variety of elastomers including 3D-printed elastomeric polyurethane (EPU), dielectric elastomer VHB 4910, commercial 3D-printed silicone (SIL30) and filled rubber Viton™ specimens under uniaxial loading – unloading deformations at various rates. It is shown that the model favourably captures the considered datasets. The mathematical simplicity of the proposed modelling framework, comparatively lower number of model parameters, and the favourable modelling and predictive results suggest that the implementation and application of this modelling framework is efficient and tractable, and merit further consideration for modelling the rate-dependant mechanical behaviour of a wider range of rubber-like materials and loading modalities.

1. Introduction

Amongst many inelastic features that elastomers may exhibit under various loading and boundary conditions, including ageing, crystallisation, damage, stress relaxation/creep, rate-dependant behaviour, softening in unloading etc., the latter two are perhaps the most frequently encountered characteristics in the mechanical function of many rubber-like soft materials. The occurrence of these two features are also commonly shared in soft tissues; rendering the study of rate-dependency and softening of particular relevance across various soft solids. In this work, therefore, we too will direct our focus on these two phenomena, primarily on modelling these behaviours using extant experimental data available in the literature.

The rate-dependency in the mechanical behaviour of rubber-like materials is a manifestation of a more general mechanical

* Corresponding author.

https://doi.org/10.1016/j.jmps.2023.105347
Received 5 April 2023; Received in revised form 10 May 2023; Accepted 1 June 2023
Available online 7 June 2023

characteristic known as *viscoelasticity*. From the modelling perspective, the *viscoelastic* behaviour of elastomers is customarily accounted for via an additive decomposition of the elastic and the viscous contributions.[1] The literature indicates numerous modelling efforts using this approach; see, e.g., the recent reviews by Xiang et al. (2020) and Ricker et al. (2023) for excellent summaries of the various existing *viscoelastic* models in the literature. In a broad classification, such models may be categorised as either phenomenological or (micro)structurally based. Seminal examples of the former include Lubliner (1985), Simo (1987), Holzapfel and Simo (1996), Reese and Govindjee (1998), Amin et al. (2006), Kumar and Lopez-Pamies (2016), while of the latter we note Bergström and Boyce (1998), Miehe and Göktepe (2005), Linder et al. (2011), Li et al. (2016), Zhou et al. (2018) and Dal et al. (2020) *inter alia*. However, despite the diversity in their numbers and types, many common traits may be identified across these models.

A first common basis in most of the current viscoelastic models is the multiplicative decomposition of the deformation gradient into the elastic and inelastic (viscous) parts, inspired by the work of Lee (1969) originally proposed in the realm of in finite strain plasticity. While mathematically unimpeded, the physical basis of such an assumption may be questionable, particularly since the decomposed so called inelastic deformation gradient may not be the gradient of a real motion, as astutely pointed out by Rajagopal and Srinivasa (2004).

A second common trait is the consideration of an evolution law for the dissipative effects, and the relevant internal variables, in those models. Except for the thermodynamics requirement that the evolution law must result in a positive dissipation rate, the choice of such governing equation(s) and the internal variable(s) is essentially a constitutive assumption, based on the judicious consideration of the user; see, e.g., the works of Hossain and co-workers (Hossain et al., (2012); Hossain and Liao (2020) and Hossain et al., (2020) amongst many other contributions from the same group) which have opted for different evolution laws for different elastomers. As a result, these evolution laws introduce an *ad hoc* level of complexity into the ensuing models – see also the recent contribution of Srikanth et al., (2023) for a summary of various models employing different evolution laws.

The third common feature in those models, partly also stemming from the foregoing trait, is the high number of additional model parameters that needs to be incorporated to account for the viscous effects. For example, the seminal micro-sphere model of Miehe and Göktepe (2005) introduces 18 viscous parameters, or the viscosity function alone in some of those models includes comparable to, or even higher than, number of parameters in a hyperelastic model; see, e.g., those of Hrapko et al., (2006) and Kumar and Lopez-Pamies (2016) with 4 and 6 parameters, respectively. The interested reader is referred to Ricker et al., (2023) and Srikanth et al., (2023) for more detailed information on various models and the additional number of viscous parameters embodied in those models. In addition to the problems that a high number of model parameters inherently poses to finding the unique optimal fit and thereby identifying unique model parameter values (Ogden et al., 2004; Destrade et al., 2017), it still remains debatable whether (micro)structural-based models which typically carry higher number of model parameters do indeed provide a better fit to some datasets compared with models that incorporate lower number of parameters (Zhou et al., 2018).

The fourth shared characteristic, as a result of the aforementioned three points, is that different models are required for satisfactorily capturing the viscoelastic deformation of different elastomers. In other words, the universal application of most, if not all, of the existing models and modelling approaches in the literature to capturing the viscoelastic behaviour of various elastomers is often handicapped and meets its limitation. Again, the work of Hossain and co-workers (e.g., Hossain et al., (2012); Liao et al., (2019); Hossain et al., (2020) and Hossain and Liao (2020) *inter alia*) on 3D-printed elastomeric polyurethane (EPU) samples, dielectric elastomer VHB 4910 specimens as well as commercial 3D-printed silicone testers exemplifies this point, as not only different evolution laws had to be considered for modelling the rate-dependant behaviour of these elastomers, but different basic hyperelastic functions were required too.

In passing we also note additional two general shortcomings of the existing viscoelastic models: (i) to the extent that the models are calibrated by fitting to the (macro-level) experimental data, (micro)structurally-based models do not offer any particular advantage over the phenomenological models; and (ii) many of the evolution laws do not result in the rate of deformation to appear as an explicit variable in the final form of the model formulation. Incorporating the deformation rate as an explicit variable in the model provides a versatile feature, since the rate of deformation is a control variable in the experiments and is provided as an input to the model. A modelling framework which facilitates such an incorporation is that devised by Maugin (1995) and Pioletti et al., (1998), which considers a 'dissipation potential' with an embedded rate of deformation, from which the additional rate-dependant stresses are derived. However, this approach seems to have been more utilised in the context of soft tissue biomechanics (see, e.g., Anssari-Benam et al., (2017; 2018; 2022b; 2023b) amongst others) and not elastomers; and therefore will not be considered here in any depth.

The foregoing complexities are further exacerbated if damage needs to be also accounted for. The particular damage feature of interest here is the softening observed in the unloading curves, akin to the Mullin's effect in natural and filled rubbers (Mullins, 1947; Harwood et al., 1965). Depending on the chosen framework as to how to model damage, the ensuing softening model can incorporate up to 14 parameters (e.g., the network evolution model by Dargazany and Itskov (2009), the network decomposition model of Dargazany and Itskov (2013), and more recent multi-network based models by Morovati and Dargazany (2019) and Morovati et al., (2021) amongst other approaches), when considering features such as the permanent set and induced anisotropy etc. While some of the recounted viscoelastic models do indeed already incorporate the damage effects, adding this feature to viscoelastic models in general is expected to further the complexity of the models and the number of model parameters.

Accordingly, here we wish to depart from the existing approaches in the literature to model the *rate-effects* and softening, by proposing a new modelling framework based on a recently proposed basic hyperelastic function by Anssari-Benam (2023a), so as to: (i)

[1] The elastic and viscous contributions are sometimes referred to as the 'equilibrium' and 'non-equilibrium' responses, respectively, in the literature.

reduce the complexities associated with the current modelling approaches, (ii) improve the accuracy of the predicted rate-dependant and softening behaviours, and (iii) provide a degree of *comprehensibility* in that the model could be applicable to various elastomer types. The impetus behind proposing this new framework stemmed from our primary investigations of modelling the *rate-effects* in elastomers, via the simple observation that when the basic hyperelastic model of interest (which will be elaborated in Section 2) was fitted to the stress – stretch data of various elastomers tested at each individual rate (e.g., data from Hossain et al., (2012) on dielectric elastomer VHB 4910 specimens and Hossain et al., (2020) on 3D printed elastomeric polyurethane (EPU) samples etc.), it favourably captured the datasets without the need of adding a 'non-equilibrium', or 'viscous', term. Naturally, the ensuing model parameter values identified at each rate were different. This observation led us to explore the possibility that there is perhaps *no* inherent need to consider an additive contribution of the 'viscous' effect(s) to the basic hyperelastic function W to model the rate effects, but rather W may simply be adapted such that the *model parameter values evolve (*i.e.*, vary) with the deformation rate*. In other words, our observations motivated the following proposition: For modelling the *rate- effects*, the *model parameters* of the basic *hyperelastic* function W may be considered to *evolve* with the *deformation rate*. Put differently, the model parameters of W may be considered as functions of the deformation rate. This approach, as will be shown in the sequel, is also easily amenable to accommodating the softening in unloading paths, through a recently proposed extension by Anssari-Benam et al., (2023a) to the original theory of pseudo-elasticity devised by Ogden and Roxburgh (1999). Therefore, the (few) softening parameters that will be introduced to the basic hyperelastic function will also become functions of the deformation rate, and vary (e.g., *evolve*) with the rate. The notion of evolving model parameters, though not explored in the context of rate-dependency, may also be traced in approaches to modelling polymer curing; e.g. in Lion and Höfer (2007) and Hossain et al., (2009a; 2009b); and polymer ageing; e.g., in Mohammadi and Dargazany (2019) and Bahrololoumi et al., (2021).

In the following we provide the theoretical and mathematical underpinnings of this modelling framework, and present our preliminary modelling results. We must emphasise at the outset that the proposed modelling approach only incorporates and captures the *rate-effects*, and *not* the wider viscoelastic behaviour.[2] However, its versatility, comprehensibility and accuracy should make a favourable case for the application of this modelling framework to the rate-dependant and softening behaviours of rubber-like materials. In proceeding towards this stated aim, we present the theoretical preliminaries and the model formulation in Section 2. In Section 3 we derive the ensuing general (Cauchy) stress – deformation relationships, and specialise the application of the model to uniaxial data and considering the evolution of the model parameter values with *rate* via a simple linear relationship. The application of the model to extant experimental datasets of a variety of elastomers obtained under uniaxial loading/unloading tests at various deformation rates is illustrated in Section 4, including 3D-printed elastomeric polyurethane (EPU) samples due to Hossain et al., (2020), dielectric elastomer VHB 4910 specimens from Hossain et al., (2012), commercial 3D-printed silicone test samples due to Hossain and Liao (2020), and that of filled rubber Viton™ specimens belonging to Wang and Chester (2018). Concluding remarks are conferred in Section 5.

2. Model formulation

The modelling framework pursued and presented in this section is constructed based on the following predicate. The core of the model consists of a basic hyperelastic strain energy function $W(\mathbf{F})$, where $\mathbf{F}$ is the deformation gradient. This function is then enhanced to incorporate the *rate* effects through judicious empirical choices that relate the *evolution of the model parameters* to the rate of deformation. That is, the *model parameters* become functions of the *rate*. Such empirical relations may be of linear, exponential, power-law etc nature. Note that here the *rate* of deformation is a *parameter* and *not* a *variable*; i.e., its value is pre-set and given in/by experiments. We refer to this enhanced W function as a *pseudo-hyperelastic* energy function, denoted by $W^r(\mathbf{F};\dot{\mathbf{F}})$, where $\dot{\mathbf{F}}$ is the time derivative of $\mathbf{F}$. The softening (in the unloading path) is then accounted for by incorporating the (directional) damage variable(s) into the said W^r function, resulting in $\widetilde{W}^r$, as will be defined in the sequel. Similar to the hyperelastic model parameters, the parameters related to damage are also considered to *evolve* with *rate* of deformation, i.e., as functions of rate. The (Cauchy) stress – stretch relationships are then derived from $\widetilde{W}^r$, to be used for fitting with and prediction of the experimental deformation data. The mathematical underpinning and derivations of this framework is presented in the following.

2.1. The basic hyperelastic strain energy function W

While within the foregoing described modelling framework the choice of the W function is not constrained to any presuppositions (see., e.g., the reviews of Steinmann et al., (2012), Dal et al., (2021), Kadapa and Mokarram (2022), Ricker and Wriggers (2023) and Zhan et al., (2023) for a summary of various hyperelastic W function choices in the literature), it is judicious to consider, as much as possible, a *comprehensive* model which provides more versatility (e.g., limited number of model parameters) and accuracy for modelling the datasets of various elastomers. One such model may be that recently proposed by Anssari-Benam (2023a) as:

[2] We are grateful to an anonymous reviewer for highlighting that inherent to our approach is the assumption of a *constant* and *homogeneous* rate of deformation across the continuum. These assumptions are not valid when a sharp local gradient of deformation rate is present, such as in a local impact or in the vicinity of a local flaw. In those cases, other modelling approaches that capture features such as plastic deformations (e.g., see Garcia-Gonzalez et al., 2015, 2017) may be required.

$$W(\mathbf{F}) = \frac{3(n-1)}{2n}\mu N\left[\frac{1}{3N(n-1)}\left(\lambda_1^{\alpha}+\lambda_2^{\alpha}+\lambda_3^{\alpha}-3\right) - \ln\left(\frac{\lambda_1^{\alpha}+\lambda_2^{\alpha}+\lambda_3^{\alpha}-3N}{3-3N}\right)\right], \tag{1}$$

where $\mathbf{F}$ denotes the deformation gradient tensor, and μ, n, N and α are model parameters with:

$$n,\ N \in \mathbb{R}^{+},\ \alpha \in \mathbb{R}, \tag{2}$$

subject to the condition of incompressibility $\lambda_1\lambda_2\lambda_3 = 1$. Note that μ is related to the infinitesimal shear modulus μ_0 via:

$$\mu = \frac{4n\mu_0}{\alpha^2}\ \frac{1-N}{1-nN}\ . \tag{3}$$

The dependence of W on $\mathbf{F}$ in (1) is through the eigenvalues of $\mathbf{F}$; i.e., the principal stretches λ_i.

The model in Eq. (1) is the one-term form of the more general multi-term form presented in Anssari-Benam (2023a), and is the *parent* to many of the existing landmark models in the literature including the neoHookean (Treloar, 1943), Mooney-Rivlin (Rivlin, 1948), Gent (Gent, 1996) and Ogden (Ogden, 1972) models (see Anssari-Benam (2023a) for demonstration). Due to this *comprehensive* parenthood, and the accurate fits that it provides to a wide range of multiaxial datasets compared with the existing models (see, e.g., Anssari-Benam (2023a; 2023b)), we consider this model here as a more inclusive representation of the basic hyperelastic behaviour of isotropic incompressible elastomers. In the special case where $\alpha = 2$, $n = 3$ and $\{n = 3,\ \alpha = 2\}$, the model in Eq. (1) reduces to those developed by Anssari-Benam and Horgan (2022), Anssari-Benam et al., (2022a) and Anssari-Benam and Bucchi (2018; 2021), respectively.

2.2. Incorporating the rate effect

In our primary investigations of modelling the *rate* effects in elastomers it was observed that the model in Eq. (1) favourably captured the stress – stretch data of various elastomers tested at each individual rate (e.g., data from Hossain et al., (2012) on dielectric elastomer VHB 4910 specimens and Hossain et al., (2020) on 3D printed elastomeric polyurethane (EPU) samples), naturally with different model parameter values identified at different rates. This observation led us to explore the possibility for devising a new modelling framework to capture the *rate* effects in which W may simply be adapted such that the *model parameters* vary (*evolve*) with deformation *rate*. Therefore, here we depart from the existing classical frameworks reviewed in Section 1, and instead consider the *rate of deformation* as a parameter (*not a variable*) in the basic hyperelastic function W.

To maintain frame-invariance, the incorporation of the deformation rate into W is considered via $\dot{\mathbf{F}}$, i.e., the time-derivative of $\mathbf{F}$; i.e.: $W^r \equiv W(\mathbf{F};\dot{\mathbf{F}})$, where we refer to W^r as a *pseudo-hyperelastic* energy function which incorporates the *rate* effects (and hence the superscript 'r'). We emphasise that $\dot{\mathbf{F}}$ here is strictly a parameter, in the same way that μ, n, N and α are, and is set in the experiments as a given. The *evolution* of the hyperelastic model parameters μ, n, N and α is then thought to depend on $\dot{\mathbf{F}}$; i.e., those parameters are considered to be functions of $\dot{\mathbf{F}}$:

$$\mu \equiv \mathscr{f}(\dot{\mathbf{F}});\ N \equiv \mathscr{g}(\dot{\mathbf{F}});\ \alpha \equiv \mathscr{h}(\dot{\mathbf{F}});\ n \equiv \mathscr{k}(\dot{\mathbf{F}}), \tag{4}$$

where $\mathscr{f}$, $\mathscr{g}$, $\mathscr{h}$ and $\mathscr{k}$ are empirical functions as yet unspecified. Explicitly, we define the dependence of W^r on $\dot{\mathbf{F}}$ via its eigenvalues $\dot{\lambda}_i$, as follows.

Since $\mathbf{F} = \text{diag}\ (\lambda_i)$, where λ_i are the principal stretches, it follows that $\dot{\mathbf{F}} = \text{diag}\ (\dot{\lambda}_i)$. The control variable in the experiments, however, is the *applied* deformation rate; i.e., the rate of deformation applied in the loading direction(s). Therefore, the $\dot{\lambda}_i$ of interest will be the one(s) in the loading direction(s) (and hence are experimentally controllable). Accordingly, we define $\mathbf{a}$ as a vector containing information in regard to the loading direction:

$$\mathbf{a} = [\delta_1, \delta_2, \delta_3]^{\mathrm{T}},\ \delta_i = \begin{cases} 1, \text{ if } i \text{ is the applied loading direction,} \\ 0, \text{ if otherwise.} \end{cases} \tag{5}$$

Using $\mathbf{a}$ in Eq. (5), tensor $\mathbf{A}$ is defined as:

$$\mathbf{A} = \ \mathbf{a} \otimes \mathbf{a}, \tag{6}$$

where $\otimes$ denotes the dyadic operator. We propose a specific measure of deformation by considering:

$$\dot{\varepsilon} = \max\{\mathbf{A}\dot{\mathbf{F}}\}, \tag{7}$$

i.e., the maximum array of the matrix $\mathbf{A}\dot{\mathbf{F}}$.

Remark 1. Note that in obtaining $\dot{\varepsilon}$ we consider the absolute value of the arrays of $[\mathbf{A}\dot{\mathbf{F}}]$. That is, if for example we are dealing with compression, where some or all of $\dot{\lambda}_i$ are negative, we consider the absolute value of $\dot{\lambda}_i$ in establishing $\dot{\varepsilon}$ from Eq. (7).

The *evolution* of the hyperelastic model parameters μ, n, N and α is now thought to depend on this measure of deformation rate, $\dot{\varepsilon}$, i.e., to be a function of $\dot{\varepsilon}$. Therefore, the generic functional form of W^r becomes:

$$\begin{aligned} W^r(\mathbf{F};\dot{\mathbf{F}}) \equiv W^r(\lambda_i;\dot{\varepsilon}) \quad = \quad & \frac{3[\mathscr{k}(\dot{\varepsilon})-1]}{2\mathscr{k}(\dot{\varepsilon})}\mathscr{f}(\dot{\varepsilon})\mathscr{g}(\dot{\varepsilon})\left\{\frac{1}{3\mathscr{g}(\dot{\varepsilon})[\mathscr{k}(\dot{\varepsilon})-1]}\left(\lambda_1^{\mathscr{k}(\dot{\varepsilon})}+\lambda_2^{\mathscr{k}(\dot{\varepsilon})}+\lambda_3^{\mathscr{k}(\dot{\varepsilon})}-3\right)\right. \\ & \left.-\ln\left(\frac{\lambda_1^{\mathscr{k}(\dot{\varepsilon})}+\lambda_2^{\mathscr{k}(\dot{\varepsilon})}+\lambda_3^{\mathscr{k}(\dot{\varepsilon})}-3\mathscr{g}(\dot{\varepsilon})}{3-3\mathscr{g}(\dot{\varepsilon})}\right)\right\}, \end{aligned} \tag{8}$$

where $\mathscr{f}$, $\mathscr{g}$, $\mathscr{k}$ and $\mathscr{n}$ in Eq. (4) have now been given as explicit functions of $\dot{\varepsilon}$; i.e., $\mathscr{f}(\dot{\varepsilon})$, $\mathscr{g}(\dot{\varepsilon})$, $\mathscr{k}(\dot{\varepsilon})$ and $\mathscr{n}(\dot{\varepsilon})$, respectively.

The specific functional forms of $\mathscr{f}$, $\mathscr{g}$, $\mathscr{k}$ and $\mathscr{n}$ may be designated empirically; however, it is natural to consider that in quasi-static deformations, where $\dot{\varepsilon}\to 0$, the basic hyperelastic model in Eq. (1) is recovered. Therefore, we require:

$$\begin{cases} \mathscr{f}(0)=\mu, \\ \mathscr{g}(0)=N, \\ \mathscr{k}(0)=\alpha, \\ \mathscr{n}(0)=n. \end{cases} \tag{9}$$

Subject to (9), any functional form may thus be considered. A specific form will be conferred later in the sequel. We end this section by emphasising that the *pseudo-hyperelastic* energy function W^r given in Eq. (8) may be used for capturing and modelling the rate effects in loading paths. To capture the softening in the unloading paths, the W^r function is extended to incorporate damage, presented in the next subsection.

2.3. Extension for capturing discontinuous damage: softening in the unloading paths

A particular softening effect of interest is the softening observed in the unloading curves of elastomers, akin to the Mullins effect (Mullins 1947; Harwood et al., 1965). Therefore, in order to capture this effect, the model in Eq. (8) must be enhanced to account for damage. Of the various approaches that may be utilised to capture damage, a versatile framework is the theory of pseudo-elasticity, pioneered by Ogden and Roxburgh (1999). Whereas this theory was originally devised to capture the *idealised* Mullins effect, in a recent work by Anssari-Benam et al., (2023a) we extended the application of the pseudo-elasticity framework to incorporate the permanent set and the induced anisotropy. The extended constitutive law proposed was:

$$\mathscr{W}(\lambda_i,\Omega)=\Omega\ \widehat{W}(\lambda_i,\Omega_i)+\phi(\Omega),\ \ i=1,2,3, \tag{10}$$

where Ω is the well-known damage parameter and is defined from the directional damage parameters Ω_i via:

$$\Omega=\frac{1}{3}\sum_i \Omega_i\left(\lambda_i,\lambda_i^{max}\right),\ \ i=1,2,3, \tag{11}$$

with λ_i^{max} denoting the maximum principal stretches in the loading directions, considered as the measure of maximum deformation. We note that in the undeformed configuration there is no damage, i.e., $\Omega_i=1$, and by definition $0<\Omega\leq 1$. Further, ϕ is a *damage function* which is a smooth function of Ω and $\phi(1)=0$. The function $\widehat{W}$ is mathematically defined as (Anssari-Benam et al., 2023a):

$$\widehat{W}(\lambda_i,\Omega_i)=\widetilde{W}+\varphi(\Omega_i)+\mathscr{w}(\lambda_i),\ \ i=1,2,3, \tag{12}$$

where $\widetilde{W}$ was referred to as the *pseudo-strain energy function* (not to be confused with the *pseudo-hyperelastic* energy function W^r defined in this work) and is constructed from the basic hyperelastic strain energy function W; i.e., that given in Eq. (1), by incorporating the damage parameters Ω_i . Note that here φ has the similar characteristics of the *damage function* ϕ in Eq. (10); i.e., is a smooth function of Ω_i (and hence Ω) and we require $\varphi(1)=0$. Finally, $\mathscr{w}(\lambda_i)$ is an arbitrary function of λ_i subjected to the following condition (Anssari-Benam et al., 2023a):

$$\frac{\partial\varphi(\Omega_i)}{\partial\lambda_i}=-\frac{\partial\mathscr{w}(\lambda_i)}{\partial\lambda_i}, \tag{13}$$

with the requirement that $\mathscr{w}(\lambda_i=1)=0$. The specific functional form of the directional damage parameters Ω_i was taken to be (Anssari-Benam et al., 2023a):

$$\Omega_i = \frac{b+2}{b+1} - \frac{1}{b+\exp\left[-c\ \left(\lambda_i^{max}-\lambda_i\right)\left(\lambda_i^{max}-1\right)\right]}, \tag{14}$$

where:

$$b, c \in \mathbb{R}^+, \tag{15}$$

i.e., are positive real-valued parameters. It is therefore of note, in view of Eqs. (11) and (14), that the damage parameter Ω is a *separable* function of the principal stretches λ_i. The specific functional form of $\widetilde{W}$was constructed as (Anssari-Benam et al., 2023a):

$$\widetilde{W} = \frac{3(n-1)}{2n}\mu N\left[\frac{1}{3N(n-1)}\left(\Gamma_1^{\alpha}+\Gamma_2^{\alpha}+\Gamma_3^{\alpha}-3\right) - \ln\left(\frac{\Gamma_1^{\alpha}+\Gamma_2^{\alpha}+\Gamma_3^{\alpha}-3N}{3-3N}\right)\right], \tag{16}$$

with:

$$\Gamma_i = \Omega_i^{\kappa}\lambda_i, \tag{17}$$

where κ is a real-valued constant; i.e., $\kappa \in \mathbb{R}$. Parameter κ may be considered as a *modulating* factor in converting the amount of damage into the amount of residual stretch. On the primary loading path $\Omega_i = 1$, and thus the $\widetilde{W}$ function in Eq. (16) reduces to the basic hyperelastic strain energy function W given in Eq. (1). Therefore, no permanent set is present for the hyperelastic material in the absence of damage. If one wishes to only model the *idealised* Mullins effect, i.e., the softening in the unloading path but with no permanent set, then the constant κ is set to zero, which renders $\Gamma_i = \lambda_i$, and there is, again, no permanent set. The explicit mathematical forms of the damage functions $\varphi(\Omega_i)$ and $\phi(\Omega)$, or indeed $\omega(\lambda_i)$, need not be specified, as these will not enter the stress-deformation relationships – see (Anssari-Benam et al., 2023a) for the detailed derivations.

Using the foregoing approach, here we devise the rate-dependant form of Eq. (10) while noting that b, c and κ now too become functions (as yet unspecified) of the measure of deformation rate $\dot{e}$; i.e.,

$$b \equiv \mathscr{b}(\dot{\mathbf{F}}) = \mathscr{b}(\dot{e});\ c \equiv \mathscr{c}(\dot{\mathbf{F}}) = \mathscr{c}(\dot{e});\ \kappa \equiv \mathscr{k}(\dot{\mathbf{F}}) = \mathscr{k}(\dot{e}), \tag{18}$$

as:

$$\mathscr{W}^r(\lambda_i, \Omega^r; \dot{e}) = \Omega^r\ \widehat{W}^r\left(\lambda_i, \Omega_i^r; \dot{e}\right) + \phi^r(\Omega^r),\ i = 1,2,3, \tag{19}$$

where all the parameters have the same standing as those in Eq. (10), with the superscript 'r' to indicate the specialisation for the incorporation of the *rate* effects. Note that here $\widehat{W}^r(\lambda_i, \Omega_i^r; \dot{e})$ is defined as:

$$\widehat{W}^r\left(\lambda_i, \Omega_i^r; \dot{e}\right) = \widetilde{W}^r\left(\lambda_i, \Omega_i^r; \dot{e}\right) + \varphi^r\left(\Omega_i^r\right) + \omega^r(\lambda_i),\ i = 1,2,3, \tag{20}$$

where $\widetilde{W}^r$ is the enhanced version of $W^r(\dot{e}; \lambda_i)$ given in Eq. (8) by incorporating the damage variable:

$$\widetilde{W}^r\left(\lambda_i, \Omega_i^r; \dot{e}\right) = \frac{3[\mathscr{b}(\dot{e})-1]}{2\mathscr{b}(\dot{e})}\mathscr{k}(\dot{e})\mathscr{g}(\dot{e})\left\{\frac{1}{3\mathscr{g}(\dot{e})[\mathscr{b}(\dot{e})-1]}\left(\mathrm{X}_1^{\mathscr{b}(\dot{e})}+\mathrm{X}_2^{\mathscr{b}(\dot{e})}+\mathrm{X}_3^{\mathscr{b}(\dot{e})}-3\right)\right.$$
$$\left.-\ln\left(\frac{\mathrm{X}_1^{\mathscr{b}(\dot{e})}+\mathrm{X}_2^{\mathscr{b}(\dot{e})}+\mathrm{X}_3^{\mathscr{b}(\dot{e})}-3\mathscr{g}(\dot{e})}{3-3\mathscr{g}(\dot{e})}\right)\right\}, \tag{21}$$

with:

$$\mathrm{X}_i = \left(\Omega_i^r\right)^{\mathscr{c}(\dot{e})}\lambda_i, \tag{22}$$

and similar to the condition in Eq. (13) we require:

$$\frac{\partial\varphi^r\left(\Omega_i^r\right)}{\partial\lambda_i} = -\frac{\partial\omega^r(\lambda_i)}{\partial\lambda_i}, \tag{23}$$

with the requirement that $\omega^r(\lambda_i = 1) = 0$. Also:

$$\Omega_i^r = \frac{\mathscr{b}(\dot{e})+2}{\mathscr{b}(\dot{e})+1} - \frac{1}{\mathscr{b}(\dot{e})+\exp\left[-\mathscr{c}(\dot{e})\ \left(\lambda_i^{max}-\lambda_i\right)\left(\lambda_i^{max}-1\right)\right]}, \tag{24}$$

such that: $\mathscr{b}(\dot{e}), \mathscr{c}(\dot{e}) > 0$. As before:

$$\Omega^r = \frac{1}{3}\sum_i \Omega_i^r,\ i = 1,2,3. \tag{25}$$

For a demonstration of the thermodynamical consistency of the constitutive law in Eq. (19) see Appendix A.

Analogous to $\mathscr{f}$, $\mathscr{g}$, $\mathscr{h}$ and $\mathscr{k}$, the functional forms of $\mathscr{k}$, $\mathscr{p}$ and $\mathscr{j}$ may too be designated empirically; however, it is again natural to consider that:

$$\begin{cases} \mathscr{k}(0) = b, \\ \mathscr{p}(0) = c, \\ \mathscr{j}(0) = \kappa\ . \end{cases} \tag{26}$$

Subject to (26), we will confer specific forms of $\mathscr{k}$, $\mathscr{p}$ and $\mathscr{j}$ later in the sequel. Again, note that the explicit mathematical forms of $\phi^r(\Omega^r)$, (Ω_i^r) and $\omega^r(\lambda_i)$ need not be specified, due to the fact that these will not appear in the stress – stretch relationships (see Appendix B). These relationships will be presented in the next Section.

3. The stress – deformation relationship

Since $\dot{\varepsilon}$ is a parameter, pre-set in the experiments, and thus *not* a variable, following the usual arguments for an incompressible isotropic material in the theory of pseudo-elasticity, the (Cauchy)stress-stretch $T-\lambda$ relationship may be derived from $\mathscr{W}^r$ given in Eq. (19) as:

$$T_i = \lambda_i \frac{\partial \mathscr{W}^r}{\partial \lambda_i} - p,\ \ i = 1,2,3, \tag{27}$$

where T_i denotes the components of the Cauchy stress, and p is the Lagrange multiplier enforcing the constraint of incompressibility. It can be shown (see Appendix B for the derivation) that Eq. (27) simplifies to:

$$T_i = \Omega^r \mathrm{X}_i \frac{\partial \widetilde{W}^r}{\partial \mathrm{X}_i} - p,\ \ i = 1,2,3, \tag{28}$$

which, in view of the $\widetilde{W}^r$ function in Eq. (21) breaks down to:

$$T_i = \Omega^r\ \frac{\mathscr{k}(\dot{\varepsilon})\mathscr{f}(\dot{\varepsilon})}{2\mathscr{k}(\dot{\varepsilon})}\ \mathrm{X}_i^{\mathscr{k}(\dot{\varepsilon})}\ \frac{\mathrm{X}_1^{\mathscr{k}(\dot{\varepsilon})} + \mathrm{X}_2^{\mathscr{k}(\dot{\varepsilon})} + \mathrm{X}_3^{\mathscr{k}(\dot{\varepsilon})} - 3\mathscr{k}(\dot{\varepsilon})\mathscr{g}(\dot{\varepsilon})}{\mathrm{X}_1^{\mathscr{k}(\dot{\varepsilon})} + \mathrm{X}_2^{\mathscr{k}(\dot{\varepsilon})} + \mathrm{X}_3^{\mathscr{k}(\dot{\varepsilon})} - 3\mathscr{g}(\dot{\varepsilon})} - p,\ \ i = 1,2,3. \tag{29}$$

Eq. (29) now furnishes the way for obtaining specific stress–stretch relationships for a deformation of interest.

Depending on the type of experimental test employed, the relationship in Eq. (29) may be adapted to incorporate the relevant boundary condition, and specialised for obtaining the explicit (Cauchy)stress – deformation $(T-\lambda)$ relationship(s). A common characterization method in investigating the rate-dependant mechanical properties of isotropic incompressible elastomers is the uniaxial (loading/unloading) test. For this deformation, say in direction 1, the principal stretches are:

$$\lambda_1 = \lambda,\ \ \lambda_2 = \lambda_3 = \lambda^{-0.5}\ . \tag{30}$$

Also, from Eq. (7) we note:

$$\dot{\varepsilon} = \dot{\lambda}\ . \tag{31}$$

In addition, since $\lambda_2 = \lambda_3 = \lambda^{-0.5} \leq 1$, i.e., $\lambda_2^{max} = \lambda_3^{max} = 1$, from Eq. (24) we find $\Omega_2^r = \Omega_3^r = 1$, so that we have:

$$\mathrm{X}_1 = \left(\Omega_1^r\right)^{\mathscr{r}(\dot{\lambda})}\lambda,\ \ \mathrm{X}_2 = \mathrm{X}_3 = \lambda^{-0.5},\ \ \Omega^r = \frac{1}{3}\left(\Omega_1^r + 2\right), \tag{32}$$

These relationships, on using Eq. (29), yield the following $T-\lambda$ relationship:

$$T_{uni} = \Omega^r \frac{\mathscr{k}(\dot{\lambda})\mathscr{f}(\dot{\lambda})}{2\mathscr{k}(\dot{\lambda})} \frac{\left(\Omega_1^r\right)^{\mathscr{f}(\dot{\lambda})\mathscr{k}(\dot{\lambda})}\lambda^{\mathscr{k}(\dot{\lambda})} + 2\lambda^{-0.5\mathscr{k}(\dot{\lambda})} - 3\mathscr{k}(\dot{\lambda})\mathscr{g}(\dot{\lambda})}{\left(\Omega_1^r\right)^{\mathscr{f}(\dot{\lambda})\mathscr{k}(\dot{\lambda})}\lambda^{\mathscr{k}(\dot{\lambda})} + 2\lambda^{-0.5\mathscr{k}(\dot{\lambda})} - 3\mathscr{g}(\dot{\lambda})} \times \left[\left(\Omega_1^r\right)^{\mathscr{f}(\dot{\lambda})\mathscr{k}(\dot{\lambda})}\lambda^{\mathscr{k}(\dot{\lambda})} - \lambda^{-0.5\mathscr{k}(\dot{\lambda})}\right]. \tag{33}$$

Remark 2. It is instructive to note that if one is only interested in modelling the rate-dependency in the loading phase, i.e., the unloading path is not investigated or the material shows negligible softening in unloading, then $\Omega^r = \Omega_i^r = 1$ and the related stress – stretch relationships can easily be recovered from Eq. (29) as:

$$T_i = \frac{\mathscr{k}(\dot{\varepsilon})\mathscr{f}(\dot{\varepsilon})}{2\mathscr{k}(\dot{\varepsilon})}\lambda_i^{\mathscr{k}(\dot{\varepsilon})} \frac{\lambda_1^{\mathscr{k}(\dot{\varepsilon})} + \lambda_2^{\mathscr{k}(\dot{\varepsilon})} + \lambda_3^{\mathscr{k}(\dot{\varepsilon})} - 3\mathscr{k}(\dot{\varepsilon})\mathscr{g}(\dot{\varepsilon})}{\lambda_1^{\mathscr{k}(\dot{\varepsilon})} + \lambda_2^{\mathscr{k}(\dot{\varepsilon})} + \lambda_3^{\mathscr{k}(\dot{\varepsilon})} - 3\mathscr{g}(\dot{\varepsilon})} - p,\ i = 1,2,3, \tag{34}$$

or, in the case of uniaxial loading, from Eq. (33) as:

$$T_{uni} = \frac{\mathscr{k}(\dot{\lambda})\mathscr{f}(\dot{\lambda})}{2\mathscr{k}(\dot{\lambda})} \frac{\lambda^{\mathscr{k}(\dot{\lambda})} + 2\lambda^{-0.5\mathscr{k}(\dot{\lambda})} - 3\mathscr{k}(\dot{\lambda})\mathscr{g}(\dot{\lambda})}{\lambda^{\mathscr{k}(\dot{\lambda})} + 2\lambda^{-0.5\mathscr{k}(\dot{\lambda})} - 3\mathscr{g}(\dot{\lambda})} \left[\lambda^{\mathscr{k}(\dot{\lambda})} - \lambda^{-0.5\mathscr{k}(\dot{\lambda})}\right]. \tag{35}$$

What remains to do now is to specify the functional forms of $\mathscr{f}$, $\mathscr{g}$, $\mathscr{h}$, $\mathscr{k}$, $\mathscr{b}$, $\mathscr{p}$ and $\mathscr{j}$. These functional dependencies in essence determine the *evolution* of the (elastic) model parameters μ, N, α, n, b, c and κ, respectively, with the deformation rate. Designating such functional dependencies, subject to conditions (9) and (26), is ultimately a matter of empirical judgement. An initial, and rather a simplified, starting point may be to consider a linear dependency:

$$\begin{cases} \mathscr{f}(\dot{\lambda}) = \mu + m_1\dot{\lambda},\ \mathscr{g}(\dot{\lambda}) = N + m_2\dot{\lambda},\ \mathscr{h}(\dot{\lambda}) = \alpha + m_3\dot{\lambda},\ \mathscr{k}(\dot{\lambda}) = n + m_4\dot{\lambda}, \\ \mathscr{b}(\dot{\lambda}) = b + m_5\dot{\lambda},\ \mathscr{p}(\dot{\lambda}) = c + m_6\dot{\lambda},\ \mathscr{j}(\dot{\lambda}) = \kappa + m_7\dot{\lambda}, \end{cases} \tag{36}$$

where for all m_i *except* for m_3 and m_7 we have $m_i > 0$, while $m_3, m_7 \in \mathbb{R}$, to comply with the *a priori* requirements set out in (2), (15) and just after (17). Note that m_1 will be a viscous damping-like parameter with units of [Pa s], while the remaining m_i are of a time nature (with units of [s]). With this choice of functional forms, the model embodies a total of 14 parameters. We note that at the limit $\dot{\lambda} = 0$, all the original model parameters are recovered. This is a useful feature, since it will allow the prediction of the *elastic* parameters from the rate-dependant modelling results identified by fitting the model to the rate data if the elastic deformation curves are not available, and/or to check the veracity of the modelling results.

For our modelling campaign, which will be demonstrated in Section 4, we consider the functional forms in Eq. (36) and substitute those into Eq. (35) to obtain the final form of our model for application to uniaxial loading-unloading data at various rates:

$$T_{uni} = \Omega^r \frac{(\mu + m_1\dot{\lambda})(\alpha + m_3\dot{\lambda})}{2(n + m_4\dot{\lambda})} \times \frac{\left(\Omega_1^r\right)^{(\alpha+m_3\dot{\lambda})(\kappa+m_7\dot{\lambda})}\lambda^{\alpha+m_3\dot{\lambda}} + 2\lambda^{-0.5(\alpha+m_3\dot{\lambda})} - 3(n + m_4\dot{\lambda})(N + m_2\dot{\lambda})}{\left(\Omega_1^r\right)^{(\alpha+m_3\dot{\lambda})(\kappa+m_7\dot{\lambda})}\lambda^{\alpha+m_3\dot{\lambda}} + 2\lambda^{-0.5(\alpha+m_3\dot{\lambda})} - 3(N + m_2\dot{\lambda})} \times \left[\left(\Omega_1^r\right)^{(\alpha+m_3\dot{\lambda})(\kappa+m_7\dot{\lambda})}\lambda^{\alpha+m_3\dot{\lambda}} - \lambda^{-0.5(\alpha+m_3\dot{\lambda})}\right], \tag{37}$$

where from Eq. (24):

$$\Omega_1^r = \frac{b + m_5\dot{\lambda} + 2}{b + m_5\dot{\lambda} + 1} - \frac{1}{b + m_5\dot{\lambda} + \exp[-(c + m_6\dot{\lambda})(\lambda^{max} - \lambda)(\lambda^{max} - 1)]}, \tag{38}$$

and from Eq. (25):

$$\Omega^r = \frac{1}{3}\left\{\frac{b + m_5\dot{\lambda} + 2}{b + m_5\dot{\lambda} + 1} - \frac{1}{b + m_5\dot{\lambda} + \exp[-(c + m_6\dot{\lambda})(\lambda^{max} - \lambda)(\lambda^{max} - 1)]} + 2\right\}. \tag{39}$$

4. Application to experimental data

As a pilot demonstration of the robustness of the proposed modelling approach in this manuscript, we consider the application of our model to rate-dependant behaviour of four distinct elastomers. The first dataset, from Hossain et al., (2020), reports on the uniaxial loading and unloading of 3D-printed elastomeric polyurethane (EPU) samples under various strain rates, including $\dot{\lambda} = 0.032\ s^{-1}$,

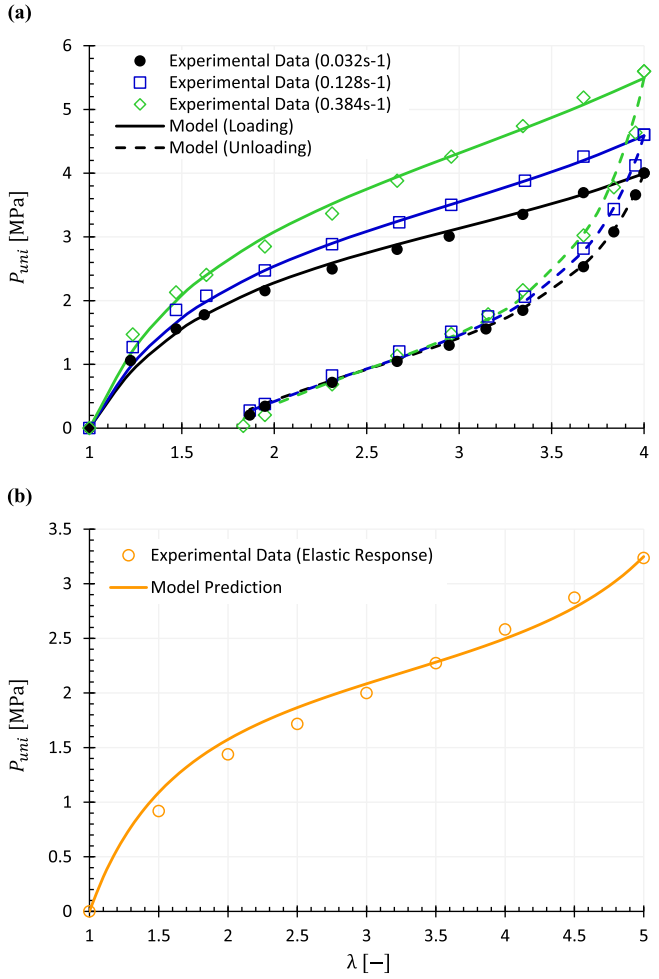

Fig. 1. Experimental nominal stress – stretch $(P-\lambda)$ data versus the model predictions for the 3D-printed elastomeric polyurethane (EPU) samples of Hossain et al., (2020) under uniaxial loading and unloading: (a) the rate-dependant deformations; and (b) the 'elastic' response. The continuous lines show the modelling results in the loading path, while the dashed lines are those of the unloading. The experimental 'elastic' response was obtained by Hossain et al., (2020) from step-wise stress-relaxation tests on the specimens. The model prediction for the elastic response was obtained by fitting the elastic version of the model to the data, using the values of μ, N, α and n in the neighbourhood identified by modelling the rate-dependant data, i.e., given in Table 1. The model parameter values for the elastic fit are: $\mu = 4.05$ [MPa], $N = 2.48$ [-], $\alpha = 1.04$ [-] and $n = 1.13$ [-].

Table 1
Model parameters for the 3D-printed EPU samples dataset due to Hossain et al., (2020).

μ [MPa]	N [-]	α [-]	n [-]	b [-]	c [-]	κ [-]
4.76	2.57	1.12	1.13	13.36	0.29	164.23
m_1 [MPa s]	m_2 [s]	m_3 [s]	m_4 [s]	m_5 [s]	m_6 [s]	m_7 [s]
3.53	1.77	-0.03	1.50	1.33×10^{-6}	0.41	8.91_5

$0.128\ s^{-1}$ and $0.384\ s^{-1}$. The second set of experimental data pertains to the uniaxial deformation of dielectric elastomer VHB 4910 specimens under various rates of $\dot{\lambda} = 0.01\ s^{-1}$, $0.03\ s^{-1}$ and $0.05\ s^{-1}$ by Hossain et al., (2012). The third dataset belongs to Hossain and Liao (2020) on using a commercial 3D-printed silicone (SIL30) by Carbon3D™, under uniaxial tests encompassing quasi-static loading-unloading experiments as well as those performed at $\dot{\lambda} = 0.01\ s^{-1}$, $0.05s^{-1}$ and $0.1\ s^{-1}$. The fourth and final dataset belongs to Wang and Chester (2018) and is related to uniaxial loading-unloading cycles of filled rubber Viton™ samples under quasi-static and $\dot{\lambda} = 0.01\ s^{-1}$ and $0.1\ s^{-1}$ loading conditions. In the following we will present the modelling results of these datasets using our proposed approach.

For the first three datasets, in keeping with the source data where the nominal stress **P** has been reported as the measure of stress,

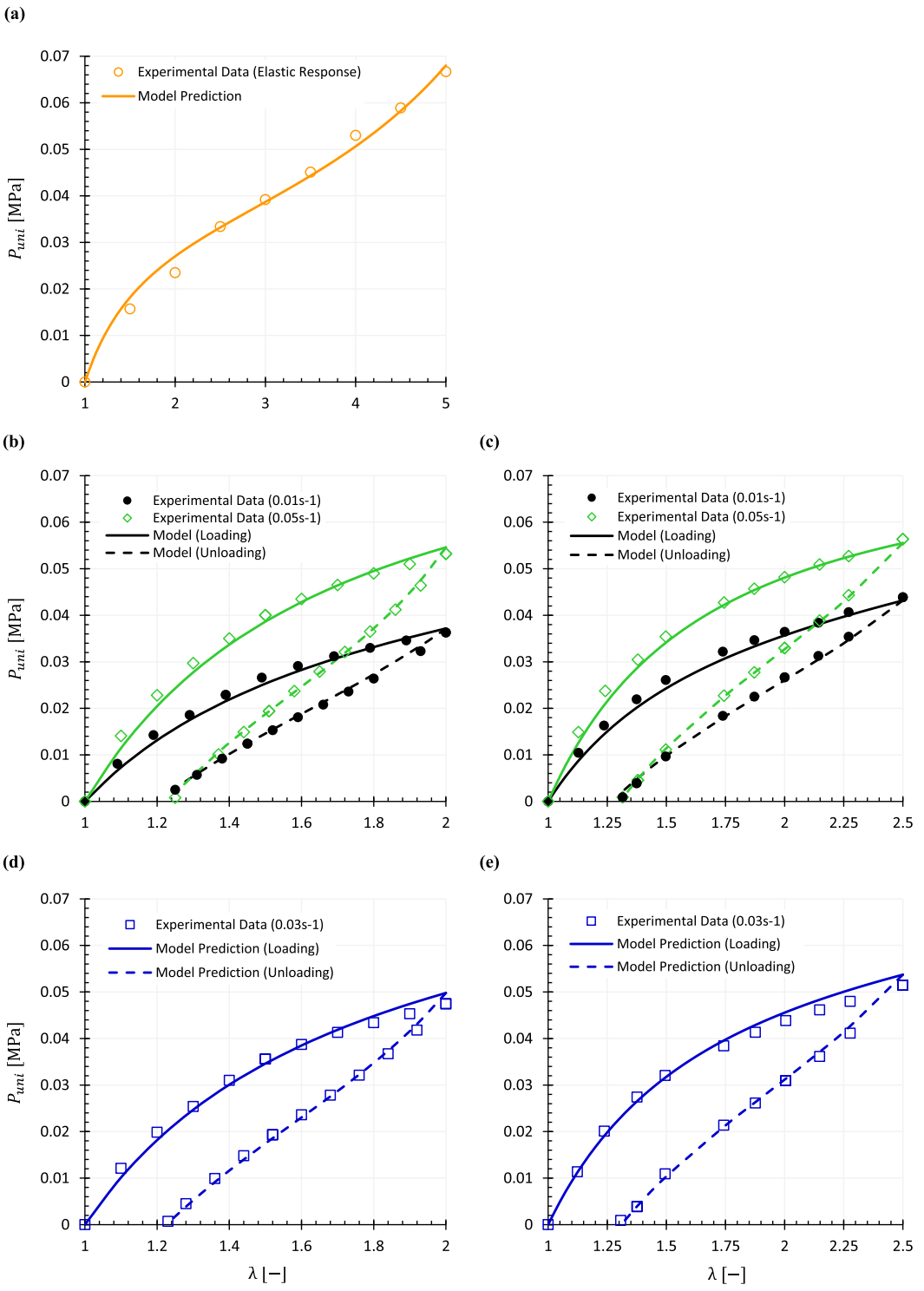

Fig. 2. Experimental nominal stress – stretch $(P-\lambda)$ data versus the modelling results for the dielectric elastomer VHB 4910 specimens due to Hossain et al., (2012): (a) the 'elastic' response (obtained from step-wise stress-relaxation tests on the specimens); (b) simultaneous fitting to the data obtained at $\dot{\lambda} = 0.01\ s^{-1}$ and $0.05\ s^{-1}$ for specimens tested up to $\lambda = 2$ (with fixed elastic parameter values); (c) simultaneous fitting to the data obtained at $\dot{\lambda} = 0.01\ s^{-1}$ and $0.05\ s^{-1}$ for specimens tested up to $\lambda = 2.5$ (with the same fixed elastic parameter values); (d) model prediction of the data at an intermediary rate $\dot{\lambda} = 0.03\ s^{-1}$ for specimens tested up to $\lambda = 2$; and (e) model prediction of the data at an intermediary rate $\dot{\lambda} = 0.03\ s^{-1}$ for specimens tested up to $\lambda = 2.5$. The continuous lines show the modelling results in the loading path, while the dashed lines are those of the unloading.

the $T-\lambda$ relationship in Eq. (37) was first converted to $P-\lambda$ relationship on using $\mathbf{T}=\mathbf{FP}$, where $\mathbf{F}$ is the deformation gradient tensor. The ensuing relationship was then fitted to the datasets, as will be specified in the sequel. For the fourth dataset, where $T-\lambda$ data has been provided, the relationship in Eq. (37) was directly fitted to the data. In each fitting exercise, the best fits were achieved by minimising the residual sum of squares (RSS) function defined as: $\mathrm{RSS}=\sum_r (P^{model}-P^{experiment})_j^2$ or $\mathrm{RSS}=\sum_r (T^{model}-T^{experiment})_j^2$, where j is the number of data points, depending on the reported experimental data as mentioned in the foregoing. The minimisations were performed via an in-house developed code in MATLAB®, using the genetic algorithm (GA) function; see, e.g., Anssari-Benam et al., (2023a).

We start by considering the data due to Hossain et al., (2020) on 3D-printed elastomeric polyurethane (EPU) samples. The converted form of Eq. (37) was fitted simultaneously to the datasets obtained at the three designated rates ($\dot{\lambda}=0.032\ s^{-1}$, $0.128\ s^{-1}$ and $0.384\ s^{-1}$). The plots in Fig. 1a present the modelling results, and Table 1 summarises the identified model parameters.

While in the original study Hossain et al., (2020) did not wish to carry out the 'elastic' loading-unloading tests, i.e., at a quasi-static loading rate, they performed step-wise stress-relaxation tests from which they constructed a loading curve portending to be the 'elastic' stress – deformation curve. The data pertaining to that curve is shown in Fig. 1b. From the modelling results in Table 1, we note that the model predicts the 'elastic' loading curve using the identified values for μ, N, α and n. Interestingly, when we undertook to fit the elastic-version of the model; i.e., with no rate and damage parameters: $T_{uni}=\frac{\mu\alpha}{2n}\frac{\lambda^\alpha+2\lambda^{-0.5\alpha}-3nN}{\lambda^\alpha+2\lambda^{-0.5\alpha}-3N}(\lambda^\alpha-\lambda^{-0.5\alpha})$, to this loading curve, in the neighbourhood of the values of μ, N, α and n as given in Table 1, a favourable fit was obtained. The resulting fit is shown in Fig. 1a (continuous line). This result further reassures that the identified model parameters via the curve fitting exercise to the rate data provide a close prediction of the expected elastic response.

Next, we consider the data due to Hossain et al., (2012) of uniaxial tests on dielectric elastomer VHB 4910 specimens under various rates of $\dot{\lambda}=0.01\ s^{-1}$, $0.03\ s^{-1}$ and $0.05\ s^{-1}$. Therein, similar to the previous dataset, they also carried out step-wise stress-relaxation tests on the specimens, from which they constructed the so-considered 'elastic' stress – deformation loading curve. To test the rigour of our modelling framework, for this dataset we employed a reverse approach in fitting the model with the data, compared with the previous dataset. That is, instead of fitting the model to the rate-dependant data first and then predict the elastic response and parameter values, here we first fitted the elastic form of the model, $T_{uni}=\frac{\mu\alpha}{2n}\frac{\lambda^\alpha+2\lambda^{-0.5\alpha}-3nN}{\lambda^\alpha+2\lambda^{-0.5\alpha}-3N}(\lambda^\alpha-\lambda^{-0.5\alpha})$, to the 'elastic' stress – deformation loading curve and identified the values of μ, N, α and n (i.e., the elastic parameter values). The fitting result is illustrated in Fig. 2a, and the elastic model parameter values are given in the top row of Table 2. Then, by fixing these parameter values, we fitted the model in Eq. (37), converted to the $P-\lambda$ form, to data pertaining to deformations of up to $\lambda=2$ at $\dot{\lambda}=0.01\ s^{-1}$ and $0.05\ s^{-1}$ rates simultaneously. The ensuing fits are presented in Fig. 2b, and the identified softening and rate parameters for this fitting are shown in the middle row of Table 2. Using the identified model parameters via these fittings, we undertook to predict the $P-\lambda$ response at the intermediary rate of $\dot{\lambda}=0.03\ s^{-1}$, and compared the prediction against the experimental data. The results are shown in Figs. 2d. For all these fits, it is observed that the modelling results are in a favourable agreement with the experimental data. To further validate the model, we also considered the data for deformations up to $\lambda=2.5$. Note that for these tests, Hossain et al., (2012) employed *different* samples, of the same material, than those used for deformations up to $\lambda=2$. Due to this inter-variability between the samples, the rate effects on the stress-strain curves of the specimens tested up to $\lambda=2.5$ are not the same as those reported in Fig. 2b for $\lambda=2$ counterparts, and thus the same rate parameter values are not valid for accurately predicting this dataset. Accordingly, we fitted the model

Table 2
Model parameters for dielectric elastomer VHB 4910 specimens due to Hossain et al., (2012). The top row indicates the parameter values for the 'elastic' data, while the middle and bottom rows contain the identified rare parameters for tests up to $\lambda=2$ and $\lambda=2.5$, respectively.

The 'elastic' deformation loading data									
μ [MPa]	N [-]			α [-]			n [-]		
0.05	2.87			0.98_5			11.36		
Specimens used in tests up to $\lambda=2$									
m_1 [MPa s]	m_2 [s]	m_3 [s]	m_4 [s]	b [-]	m_5 [s]	c [-]	m_6 [s]	κ [-]	m_7 [s]
2.98	8.79	-4.11	9.99	12.04_5	41.29	0.99	45.39	67.45	79.82
Specimens used in tests up to $\lambda=2.5$									
m_1 [MPa s]	m_2 [s]	m_3 [s]	m_4 [s]	b [-]	m_5 [s]	c [-]	m_6 [s]	κ [-]	m_7 [s]
2.75	9.95	-4.51_5	9.79	9.62	67.62	0.21	12.06	95.34	2.55

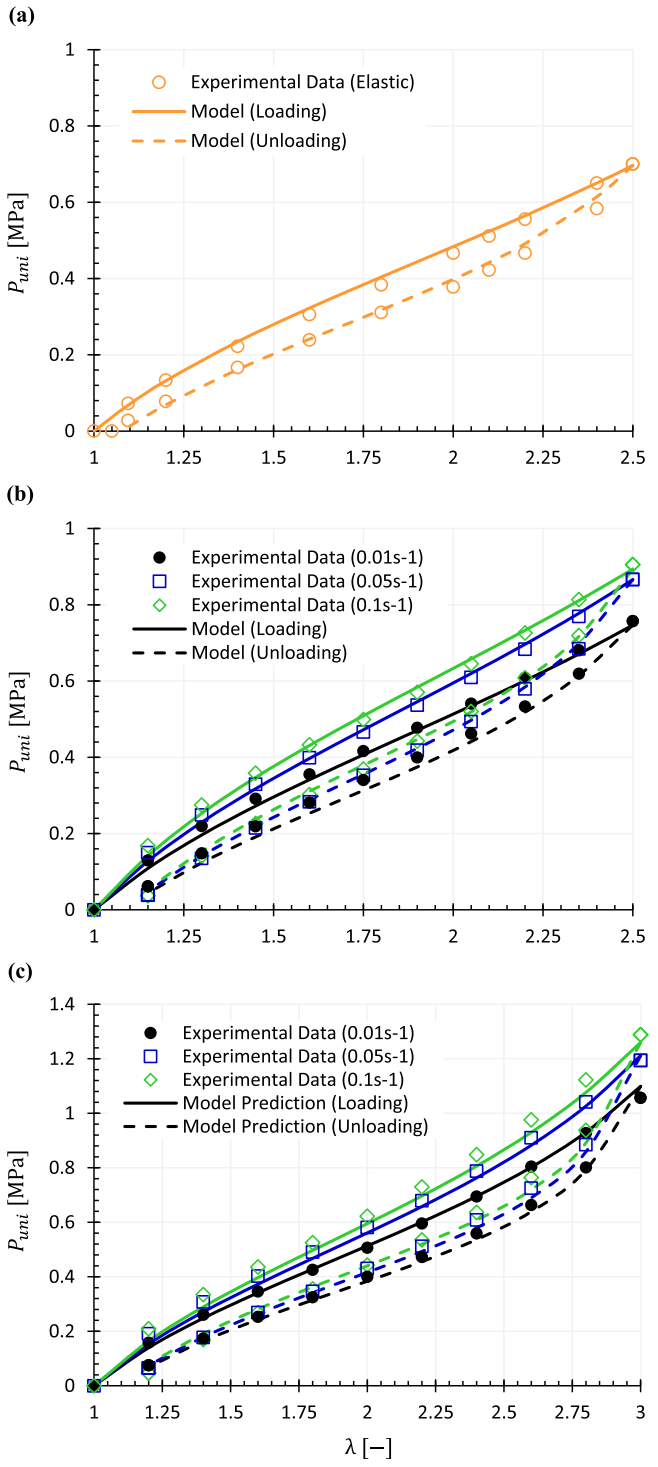

Fig. 3. Experimental nominal stress – stretch $(P-\lambda)$ data versus the modelling predictions for commercial 3D-printed silicone (SIL30) samples due to Hossain and Liao (2020): (a) the 'elastic' response (up to $\lambda = 2.5$); and (b) the rate data obtained under $\dot{\lambda} = 0.01\ s^{-1}$, $0.05\ s^{-1}$ and $0.1\ s^{-1}$ (up to $\lambda = 2.5$ deformation). These fits were obtained by simultaneously fitting Eqs. (40) and (37) to the data. (c) The *predicted* $P-\lambda$ behaviour at $\dot{\lambda} = 0.01\ s^{-1}$, $0.05\ s^{-1}$ and $0.1\ s^{-1}$ for deformations up to $\lambda = 3$ using the identified model parameters obtained by the simultaneous fits (a) and (b), given in Table 3, versus the experimental data. The continuous lines show the modelling results in the loading path, while the dashed lines are those of the unloading.

Table 3
Model parameters for the commercial 3D-printed silicone (SIL30) samples due to Hossain and Liao (2020).

μ [MPa]	N [-]	α [-]	n [-]	b [-]	c [-]	κ [-]
0.23_5	5.12	2.06	1.21	18.63	1.43	43.41
m_1 [MPa s]	m_2 [s]	m_3 [s]	m_4 [s]	m_5 [s]	m_6 [s]	m_7 [s]
1.75	0.02	-2.94	10.00	10^{-6}	9.99	9.99

in Eq. (37) again simultaneously to datasets obtained at $\dot{\lambda} = 0.01\ s^{-1}$ and $0.05\ s^{-1}$ rates for the tested specimens of up to $\lambda = 2.5$, with the same fixed values of the elastic parameters μ, N, α and n. The plots in Figs. 2c show the fitting results, and the bottom row of Table 2 summarises the identified softening and rate parameter values. Using the identified model parameters via this exercise, we again predicted the $P - \lambda$ response at the intermediary rate of $\dot{\lambda} = 0.03\ s^{-1}$ and compared it with the experimental data. The results are shown in Figs. 2e. Reassuringly, the model predictions are in close affinity with the experimental data. It is therefore observed that the model facilitates favourable predictions of the *rate*-dependant behaviour from the elastic deformation response.

We now present the modelling results of the rate data due to Hossain and Liao (2020) for a commercial 3D-printed silicone (SIL30) by Carbon3D™. In that study the authors also report the 'elastic' loading-unloading curve, obtained at a quasi-static rate of $\dot{\lambda} = 0.0005\ s^{-1}$, as well as the deformation data obtained under $\dot{\lambda} = 0.01\ s^{-1}$, $0.05\ s^{-1}$ and $0.1\ s^{-1}$. The quasi-static data was fitted to the non-rate version of the model (i.e., when $\dot{\lambda} = 0$ as developed in Anssari-Benam et al., 2023a), having the form:

$$T_{uni} = \Omega\ \frac{\alpha\mu}{2n}\ \frac{\lambda^{\alpha}\Omega_1^{\alpha\kappa} + 2\lambda^{-0.5\alpha} - 3nN}{\lambda^{\alpha}\Omega_1^{\alpha\kappa} + 2\lambda^{-0.5\alpha} - 3N}\ \left(\lambda^{\alpha}\Omega_1^{\alpha\kappa} - \lambda^{-0.5\alpha}\right), \tag{40}$$

where:

$$\Omega_1 = a - \frac{1}{b + \exp[-c\ (\lambda^{max} - \lambda)(\lambda^{max} - 1)]}, \tag{41}$$

and:

$$\Omega = \frac{1}{3}(\Omega_1 + 2), \tag{42}$$

simultaneously with the rate data using Eq. (37). In this way, the identified 'elastic' model parameters (i.e., μ, N, α, n, b, c and κ) remain constant also in modelling the rate data. The results are presented in Fig. 3a and 3b, and Table 3 summarises the identified model parameters. Note that the specimens were tested up to $\lambda = 2.5$. The favourable correlation between the data and modelling predictions is evident.

Equipped with these results, we undertook to predict the $P - \lambda$ response from the identified model parameters in Table 3 for deformations up to $\lambda = 3$, and compared it with the reported data of Hossain and Liao (2020). The predictions are shown in Fig. 3c. It is observed that the model favourably predicts the rate behaviour even beyond the initial range by which it was calibrated with ($\lambda = 2.5$).

Finally, we consider here the uniaxial loading-unloading data of Wang and Chester (2018), where they report the $T - \lambda$ curves for their Viton™ samples. Therein they carried out loading-unloading tests on the specimens for three successive cycles at quasi-static as well as $\dot{\lambda} = 0.01\ s^{-1}$ and $0.1\ s^{-1}$ rates. Similar to the previous dataset, we fitted this dataset simultaneously to the non-rate version of the model (i.e., when $\dot{\lambda} = 0$) as given by Eq. (40) with Ω_1 and Ω defined in Eqs. (41) and (42), respectively, and the rate-dependant form of the model as given by Eq. (37). We emphasise again that in this way the identified 'elastic' model parameters (i.e., μ, N, α, n, b, c and κ) remain constant also in modelling the rate data, as one would expect, so that only the rate-dependant *evolution* parameters can vary. The modelling results are shown in Fig. 4. The identified model parameters have been given in Table 4.

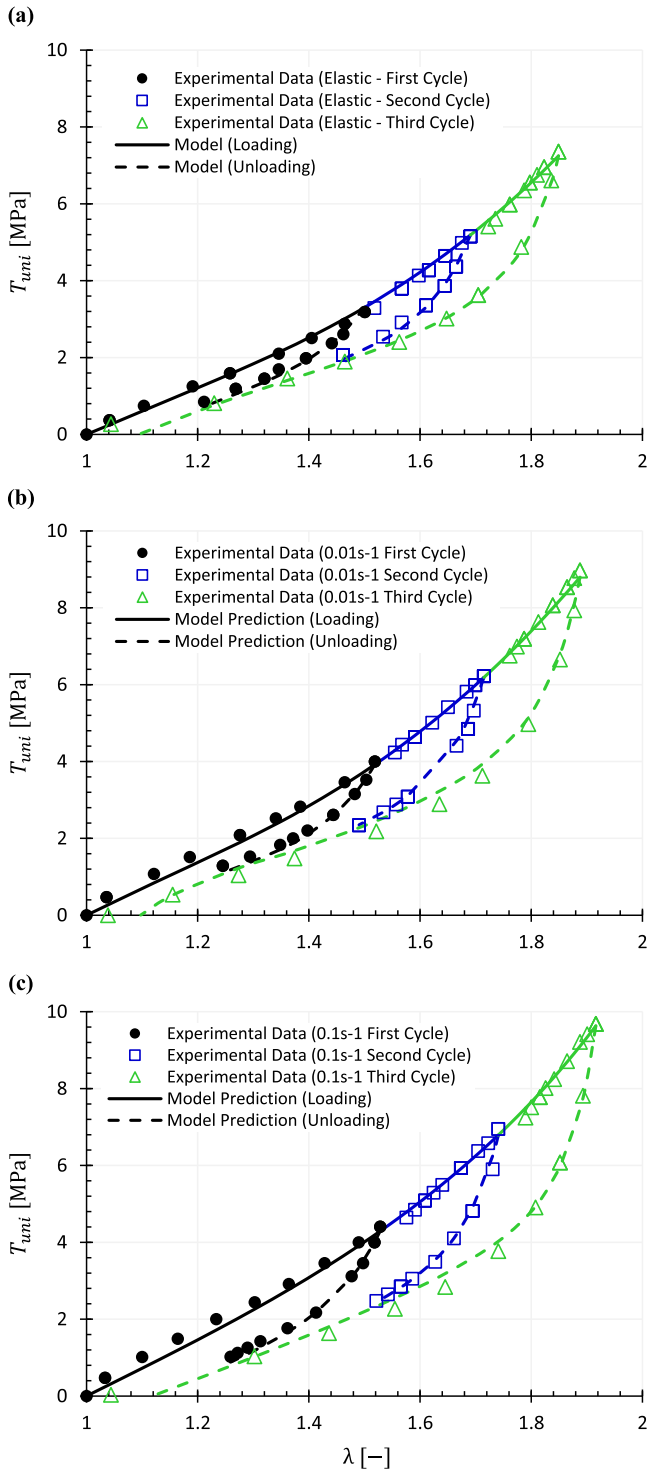

Fig. 4. Modelling results for the experimental Cauchy stress – stretch $(T-\lambda)$ data of Viton™ specimens due to Wang and Chester (2018): (a) the elastic loading-unloading cycles; (b) the loading-unloading cycles at $\dot{\lambda} = 0.01\,s^{-1}$; and (c) the loading-unloading cycles at $\dot{\lambda} = 0.1\,s^{-1}$. The continuous lines show the modelling results in the loading path, while the dashed lines are those of the unloading. The elastic and rate data were simultaneously fitted to Eqs. (40) and (37), respectively.

Table 4
Model parameters for the commercial Viton™ samples due to Wang and Chester (2018).

μ [MPa]	N [-]	α [-]	n [-]	b [-]	c [-]	κ [-]
0.25	0.64	3.80	0.71	10.73	15.90	16.88
m_1 [MPa s]	m_2 [s]	m_3 [s]	m_4 [s]	m_5 [s]	m_6 [s]	m_7 [s]
19.23	14.98	-20.95	18.12	14.80	3.79×10^{-5}	101.23

5. Remarks for discussion and conclusion

The current work aimed to present the case for a new framework to model the *rate-dependant* mechanical behaviour of elastomers, both in loading and unloading (e.g., with softening) paths. For doing so, the relative simplicity of the model (via only an extension to the basic hyperelastic modelling), its thermodynamics consistency, and the accurate modelling results with relatively low number of model parameters were illustrated. The presented modelling framework departs from the classical approach of considering an additive contribution of the so called non-equilibrium, or viscous, part to the elastic response. Instead, the model parameters of the basic hyperelastic function are thought to vary, or *evolve*, with the deformation rate, and that *evolution* is incorporated into the model. Based on this framework, a specific basic hyperelastic function W was utilised, and specialised to incorporate the deformation *rate* and softening effects. The devised model was then applied to deformation datasets obtained from various elastomers, from dielectric elastomers to 3D-printed silicone samples and filled-rubber specimens. The preliminary results presented here indicate that the model favourably captures the data, even with the rather simplistic linear *evolution* relationships between the model parameters and the rate of deformation. In addition, the proposed modelling approach allows for the rate of deformation to be present as an explicit variable in the model; a feature that is not shared with many of the existing models in the literature.

We note, however, that while the foregoing encouraging results provide a reassuring platform for further investigation of the comprehensibility and applicability of the proposed model for a broader set of elastomers, its suitability for application to a wider range of deformation rates (e.g., to higher deformation rates than those considered here) and multi-modal deformations (e.g., not only uniaxial) remains to be tested. This premise will be pursued in a follow up study. We also note the inherent empirical nature of the *evolution* relationships that characterise the variation of the model parameter values with rate in this framework. While considering more elaborate nonlinear relations such as power-law etc. may improve the modelling results, it will introduce a higher number of model parameters compared with the linear relationship considered here. Even in that case, however, the overall number of model parameters will still be comparable with the existing models in the literature, some of which alluded to in Section 1. It may also be informative to note that, as the results of Mao et al., (2017) and Hossain et al., (2020) amongst many others indicate, the softening in the unloading path of some elastomers may mainly be driven by the maximum deformation reached in the preceding loading cycle rather than the deformation rate, since the unloading paths of specimens loaded to the same deformation at different rates largely coincide (except for the initial difference between the stress levels), and the permanent sets also remain unaltered. Such results indicate that the softening parameters may be rate-insensitive, and hence there may not be any need for considering those parameters to evolve with rate. Should this prove to be the case, it will reduce the number of model parameters further.

Further, it is instructive to recall that the presented modelling approach here is specific to only capturing the deformation *rate* effects, and *not* the broader viscoelastic behaviour such as the stress-relaxation and/or creep phenomena. On occasions where modelling the stress-relaxation behaviour of the subject elastomer is desired, the internal variable evolution models appear to be the preferred choice. However, we caution the reader on the usefulness of stress-relaxation tests and the extent of applicability of stress-relaxation in the functioning environment of elastomers. For example, it is well known that for truly separating the nonlinear elastic and time-dependant viscoelastic behaviours, an instantaneous step displacement should be applied in stress-relaxation tests onto the specimen. However, since mechanical testing devices are only capable of applying a ramp displacement, the specimen immediately begins to relax by some unknown amount during this phase, particularly if the displacement ramp is applied over a finite time. Therefore, the relaxation measured during the hold phase is in effect a reduced version of the actual relaxation, to the extent of the relaxation amount during the ramp loading phase (Doehring et al., 2004). This discrepancy naturally leads to erroneous parameter estimation from the relaxation tests. As another example, if the functional loading (and unloading) of elastomeric components that operate under high working deformation rates, or equivalently are tested under high deformation rates, occurs at a fast-enough rate so that the actual amount of relaxation experienced by the components is negligible, then reliance on stress-relaxation behaviour to calibrate a model for capturing the rate effects in those elastomers may be deemed superfluous.

Finally, we note that the basic hyperelastic model considered here, i.e., that in Eq. (1), is of the limiting extensibility type for when $N > 0$; see Anssari-Benam (2023a). This feature means that the model will predict a rapid hardening as the deformation stretch approaches the limit. Due to the inherent nonlinear nature of the model and the minimisation process (i.e., fitting with the experimental data), if the model is calibrated on using stress – stretch data of lower amount of deformation, one cannot reliably expect an accurate estimation of the stress – stretch curve for higher levels of deformation using the same identified model parameters. See Appendix B of Anssari-Benam et al., (2021) for a discussion and numerical demonstrations of this point on using a sub-class of the same family of models. This feature is common to all models with a limiting chain extensibility characteristic, as well as models that when applied to the data result in a high value of the exponent(s) of the principal stretches such as, for example, the Ogden (1972) model. Therefore, a methodical way to calibrate the proposed model is to perform quasi-static deformation tests up to the highest level of deformation (stretch) possible, and simultaneously fit the model to this data as well as the data obtained from deformations at various rates.

Alternatively, if quasi-static tests are not carried out, the tests at various rates must be performed to the highest achievable level of deformation (stretch), and the model be calibrated by simultaneous fitting to those datasets at various rates. The identified model parameters in this way can then be used for predicting the deformation behaviour of the subject specimen at other rates (high or low), up to the deformation levels used for calibrating the model.

CRediT authorship contribution statement

Afshin Anssari-Benam: Conceptualization, Methodology, Writing – original draft, Investigation. **Mokarram Hossain:** Conceptualization, Writing – review & editing.

Declaration of Competing Interest

The authors declare no competing interests.

Data availability

The datasets used in support of the findings of this manuscript are obtainable from the corresponding author upon reasonable request.

Appendix A. Thermodynamical consistency of the constitutive law in Eq. (19)

A thermodynamical axiom for assessing the validity of any given constitutive relationship is its compliance with the second law of thermodynamics. Within the framework of continuum mechanics, a convenient manifestation of this law is considered through the Clausius-Duhem inequality which stipulates that the rate of dissipation in any deformation described by a proposed constitutive law must be non-negative. Assuming isothermal deformations, Naumann and Ihlemann (2015) have brilliantly analysed the compliance of the original pseudo-elasticity theory (of Ogden and Roxburgh, 1999) with this inequality. Adopting their approach, here we briefly demonstrate the thermodynamics validity of our proposed constitutive law in Eq. (19).

Considering only the mechanical contributions (i.e., discounting the temperature and heat transfer effects etc.), the Clausius-Duhem inequality reads (Naumann and Ihlemann, 2015):

$$\mathfrak{D} := \frac{1}{2}\mathbf{S} : \dot{\mathbf{C}} - \dot{W} \geq 0, \tag{A1}$$

where $\mathfrak{D}$ is the rate of dissipation per unit volume, W is the free energy (e.g., from which the stresses are derived), $\dot{W}$ is its time derivative, $\mathbf{S}$ and $\dot{\mathbf{C}}$ are the 2nd Piola-Kirchhoff and the time-derivative of the right Cauchy-Green tensors, respectively, and the operator (:) is 'double contraction'. Within the context of the current work, the free energy of concern is $\mathscr{W}^{\mathscr{T}}$given by Eq. (19). Accordingly, we must have:

$$\mathfrak{D} := \frac{1}{2}\mathbf{S} : \dot{\mathbf{C}} - \dot{\mathscr{W}}^{\mathscr{T}} \geq 0, \tag{A2}$$

with:

$$\dot{\mathscr{W}}^{\mathscr{T}} = \frac{\mathrm{d}\,\mathscr{W}^{\mathscr{T}}}{\mathrm{d}t} = \frac{\partial \mathscr{W}^{\mathscr{T}}}{\partial \mathbf{C}} : \frac{\partial \mathbf{C}}{\partial t} + \frac{\partial \mathscr{W}^{\mathscr{T}}}{\partial \Omega^r} \cdot \frac{\partial \Omega^r}{\partial t} \ . \tag{A3}$$

Recall from Section 3 that $\mathscr{W}^{\mathscr{T}} \equiv \mathscr{W}^{\mathscr{T}}(\mathbf{F}, \Omega^r; \dot{\mathbf{F}})$; i.e., $\dot{\mathbf{F}}$ is a parameter in $\mathscr{W}^{\mathscr{T}}$ and not a variable, set to a specified value in experiments, and hence the chain rule in the right-hand side of Eq. (A3). By substituting $\frac{\partial \mathbf{C}}{\partial t}$ and $\frac{\partial \Omega^r}{\partial t}$ in Eq. (A3) with the familiar notations $\dot{\mathbf{C}}$ and $\dot{\Omega}^r$, respectively, and inserting into (A2) we get:

$$\mathfrak{D} := \frac{1}{2}\mathbf{S} : \dot{\mathbf{C}} - \left(\frac{\partial \mathscr{W}^{\mathscr{T}}}{\partial \mathbf{C}} : \dot{\mathbf{C}} + \frac{\partial \mathscr{W}^{\mathscr{T}}}{\partial \Omega^r} \dot{\Omega}^r \right) \geq 0 \ . \tag{A4}$$

However, by definition (see Appendix B):

$$\frac{\partial \mathscr{W}^{\mathscr{T}}}{\partial \Omega^r} = 0, \tag{A5}$$

which renders the inequality in (A4) as:

$$\mathfrak{D} := \left(\frac{1}{2}\mathbf{S} - \frac{\partial \mathscr{W}^{\mathscr{T}}}{\partial \mathbf{C}} \right) : \dot{\mathbf{C}} \geq 0 \ . \tag{A6}$$

This inequality is *a priori* satisfied since the 2nd Piola-Kirchhoff tensor is derived from the free energy $\mathscr{W}^r$ by definitona as:

$$\mathbf{S} = 2\frac{\partial \mathscr{W}^r}{\partial \mathbf{C}} \ . \tag{A7}$$

Therefore, the proposed constitutive law in Eq. (19) is in compliance with the Clausius-Duhem inequality in that the ensuing dissipation is non-negative.

However, as noted by Naumann and Ihlemann (2015), it is somewhat counter-intuitive to consider the softening in the unloading path as a non-dissipative phenomenon (i.e., $\mathfrak{D} = 0$). To the contrary, it is reasonable to expect a positive dissipation. In their original paper, Ogden and Roxburgh (1999) defined a *dissipation rate* parameter, derived from the *non-recoverable* (or *residual*) part of the energy, and showed that this rate was always positive. Employing their approach here, it can be shown that the same finding also applies to the constitutive law in Eq. (19). Accordingly, when the continuum returns to a fully unloaded (i.e., $\lambda_i = 1$) configuration, we have from Eq. (19) that:

$$\mathscr{W}^r = \Omega^r \times 0 + \phi^r\left(\Omega^r_{min}\right) = \phi^r\left(\Omega^r_{min}\right), \tag{A8}$$

where we note that $X_i = \lambda_i$ since there has been no permanent set and thus $\widehat{W}^r = 0$, akin to a non-deformed state, and that the damage variable Ω^r by definition attains its minimum value Ω^r_{min}. The residual value $\phi^r(\Omega^r_{min})$ is referred to as the *non-recoverable* part of the energy $\mathscr{W}^r$; i.e., the part that is lost due to dissipation. Now, by definition $\frac{\partial \mathscr{W}^r}{\partial \Omega^r} = 0$, and thus from Eq. (19) we get:

$$\frac{\partial \mathscr{W}^r}{\partial \Omega^r} = 0 \Rightarrow \widehat{W}^r + \Omega^r \frac{\partial \widehat{W}^r}{\partial \Omega^r} + \frac{\partial \phi^r}{\partial \Omega^r} = 0, \tag{A9}$$

which, in view of the fact that $\frac{\partial \widehat{W}^r}{\partial \Omega^r} = 0$ (see, e.g., Appendix B) results in:

$$\widehat{W}^r = -\frac{\partial \phi^r}{\partial \Omega^r} = -\phi^{r'}, \tag{A10}$$

where the notation $\phi^{r'}$ has been introduced for $\frac{\partial \phi^r}{\partial \Omega^r}$. Since the maximum value of energy $\widehat{W}^r_{max}$ occurs at the maximum deformation point before the unloading initiates; i.e., when $\Omega^r = 1$, we obtain from Eq. (A10):

$$\widehat{W}^r_{max} = -\phi^{r'}(1). \tag{A11}$$

As pointed out by Ogden and Roxburgh (1999), Eq. (A11) indicates that function ϕ^r, through $\widehat{W}^r_{max}$, depends on the point at which the unloading initiates. Similar to Ogden and Roxburgh (1999), then, let us define an arbitrary function $f(\Omega^r)$ that accounts for this feature:

$$f(\Omega^r) = \phi^{r'}(\Omega^r) + \widehat{W}^r_{max} = \phi^{r'}(\Omega^r) - \phi^{r'}\ (1) \Rightarrow \phi^{r'}(\Omega^r) = f(\Omega^r) + \phi^{r'}\ (1)\ . \tag{A12}$$

By integrating both sides of the above ansatz with respect to Ω^r we get:

$$\phi^r(\Omega^r) = \int_1^{\Omega^r} f(\Omega^r)\mathrm{d}\Omega^r + (1-\Omega^r)\widehat{W}^r_{max}, \tag{A13}$$

and to obtain the non-recoverable part of energy in Eq. (A8), we insert $\Omega^r = \Omega^r_{min}$:

$$\phi^r\left(\Omega^r_{min}\right) = \int_1^{\Omega^r_{min}} f(\Omega^r)\mathrm{d}\Omega^r + \left(1-\Omega^r_{min}\right)\widehat{W}^r_{max}\ . \tag{A14}$$

By differentiating the above equation with respect to time we find:

$$\dot{\phi^r}(\Omega^r_{min}) = (1-\Omega^r_{min})\dot{\widehat{W}^r_{max}} \tag{A15}$$

Since by definition $0 < \Omega^r \leq 1$, it is clear that $(1-\Omega^r_{min}) \geq 0$. In addition, since stress is increasing with deformation (up to the failure point), it follows that $\widehat{W}^r_{max}$ is also increasing with deformation and thus $\dot{\widehat{W}^r_{max}} > 0$. Therefore, $\dot{\phi^r}(\Omega^r_{min}) \geq 0$, meaning that the rate of dissipation is always non-negative.

It is thus observed that on using either the Clausius-Duhem inequality approach of Naumann and Ihlemann (2015) or the energy argument of Ogden and Roxburgh (1999), the constitutive law in Eq. (19) is consistent with the requirements of the second law of thermodynamics, in that the ensuing dissipation rate is always non-negative.

Appendix B. Derivation of the (Cauchy)stress-stretch $T-\lambda$ relationship in Eq. (27)

Since $\dot{\varepsilon}$ is a parameter, with a given fixed value in experiments, the damage parameter Ω^r is only a function of the deformation gradient $\mathbf{F}$ as its *variable*. Let $\mathscr{F}$ denote an arbitrary function which constrains Ω^r to $\mathbf{F}$ as (Ogden, 2001):

$$\mathscr{F}(\mathbf{F},\Omega^r)=0\ . \tag{B1}$$

Since $\mathscr{F}$ is an arbitrary function, and the dependence of $\mathscr{W}^r$ on Ω^r is also arbitrary, one solution is obtained if $\mathscr{F}$ is set to be: $\mathscr{F}=\frac{\partial\mathscr{W}^r}{\partial\Omega^r}$. It follows from Eq. (B1) that:

$$\frac{\partial\mathscr{W}^r(\lambda_i,\Omega^r;\dot{\varepsilon})}{\partial\Omega^r}=0\ . \tag{B2}$$

Note that the dependence of $\mathscr{F}$ on $\mathbf{F}$ has been taken via the eigenvalues of $\mathbf{F}$, i.e., the principal stretches λ_i. From the definition of Ω^r in Eq. (24) we note that $\frac{\partial\Omega^r}{\partial\Omega_i^r}=\frac{1}{3}$. Therefore, Eq. (B2) yields:

$$\frac{\partial\mathscr{W}^r(\lambda_i,\Omega^r;\dot{\varepsilon})}{\partial\Omega_i^r}=0\ . \tag{B3}$$

Similarly, the dependence of Ω_i^r on $\mathbf{F}$ may be taken to be characterised by:

$$\mathscr{F}_i\left(\mathbf{F},\Omega_i^r\right)=0,\ \ i=1,2,3, \tag{B4}$$

where $\mathscr{F}_i$ are also arbitrary functions relating Ω_i^r to $\mathbf{F}$. Again, setting $\mathscr{F}_i=\frac{\partial\widehat{W}^r}{\partial\Omega_i^r}$ renders a possible solution, and leads to:

$$\frac{\partial\widehat{W}^r\left(\lambda_i,\Omega_i^r;\dot{\varepsilon}\right)}{\partial\Omega_i^r}=0\ . \tag{B5}$$

Given that $\frac{\partial\Omega^r}{\partial\Omega_i^r}=\frac{1}{3}$, we get:

$$\frac{\partial\widehat{W}^r\left(\lambda_i,\Omega_i^r;\dot{\varepsilon}\right)}{\partial\Omega^r}=0\ . \tag{B6}$$

On using Eq. (19) we find that:

$$\begin{aligned}\frac{\partial\mathscr{W}^r(\lambda_i,\Omega^r;\dot{\varepsilon})}{\partial\lambda_i}&=\frac{\partial}{\partial\lambda_i}\left[\Omega^r\ \widehat{W}^r\left(\lambda_i,\Omega_i^r;\dot{\varepsilon}\right)+\phi^r(\Omega^r)\right]\\&=\frac{\partial\Omega^r}{\partial\lambda_i}\widehat{W}^r\left(\lambda_i,\Omega_i^r;\dot{\varepsilon}\right)+\Omega^r\frac{\partial\widehat{W}^r\left(\lambda_i,\Omega_i^r;\dot{\varepsilon}\right)}{\partial\lambda_i}+\frac{\partial\phi^r(\Omega^r)}{\partial\lambda_i}\ .\end{aligned} \tag{B7}$$

From Eq. (B2):

$$\begin{aligned}\frac{\partial\mathscr{W}^r(\lambda_i,\Omega^r;\dot{\varepsilon})}{\partial\Omega^r}=\ 0\ \ &\Rightarrow\frac{\partial}{\partial\Omega^r}\left[\Omega^r\ \widehat{W}^r\left(\lambda_i,\Omega_i^r;\dot{\varepsilon}\right)+\phi^r(\Omega^r)\right]=0\\&\Rightarrow\widehat{W}^r\left(\lambda_i,\Omega_i^r;\dot{\varepsilon}\right)+\Omega^r\frac{\partial\widehat{W}^r\left(\lambda_i,\Omega_i^r;\dot{\varepsilon}\right)}{\partial\Omega^r}+\frac{\partial\phi^r(\Omega^r)}{\partial\Omega^r}=0,\end{aligned} \tag{B8}$$

which in view of Eq. (B6) results in:

$$\widehat{W}^r\left(\lambda_i,\Omega_i^r;\dot{\varepsilon}\right)+\frac{\partial\phi^r(\Omega^r)}{\partial\Omega^r}=0\Rightarrow\frac{\partial\phi^r(\Omega^r)}{\partial\Omega^r}=-\ \widehat{W}^r\left(\lambda_i,\Omega_i^r;\dot{\varepsilon}\right)\ . \tag{B9}$$

Applying the chain rule to Eq. (B9) we obtain:

$$\frac{\partial\Omega^r}{\partial\lambda_i}=-\frac{1}{\widehat{W}^r\left(\lambda_i,\Omega_i^r;\dot{\varepsilon}\right)}\cdot\frac{\partial\phi^r(\Omega^r)}{\partial\lambda_i}\ . \tag{B10}$$

Substituting for $\frac{\partial\Omega^r}{\partial\lambda_i}$ from Eq. (B10) into Eq. (B7) yields:

$$\frac{\partial\mathscr{W}^r(\lambda_i,\Omega^r;\dot{\varepsilon})}{\partial\lambda_i}=\Omega^r\frac{\partial\widehat{W}^r\left(\lambda_i,\Omega_i^r;\dot{\varepsilon}\right)}{\partial\lambda_i}\ . \tag{B11}$$

However, we note from the condition in Eq. (23) that: $\frac{\partial\varphi^r(\Omega_i^r)}{\partial\lambda_i}=-\frac{\partial\omega^r(\lambda_i)}{\partial\lambda_i}$, which in view of Eq. (B11) implies:

$$\frac{\partial \widehat{W}^r\left(\lambda_i,\Omega_i^r;\dot{\varepsilon}\right)}{\partial\lambda_i}=\frac{\partial\left[\widetilde{W}^r\left(\lambda_i,\Omega_i^r;\dot{\varepsilon}\right)+\varphi^r\left(\Omega_i^r\right)+\omega^r(\lambda_i)\right]}{\partial\lambda_i}=\frac{\partial\widetilde{W}^r\left(\lambda_i,\Omega_i^r;\dot{\varepsilon}\right)}{\partial\lambda_i}\ . \tag{B12}$$

Using the chain rule again we find:

$$\frac{\partial\widetilde{W}^r\left(\lambda_i,\Omega_i^r;\dot{\varepsilon}\right)}{\partial\lambda_i}=\frac{\partial\widetilde{W}^r\left(\lambda_i,\Omega_i^r;\dot{\varepsilon}\right)}{\partial \mathrm{X}_i}\cdot\frac{\partial \mathrm{X}_i}{\partial\lambda_i}=\left(\Omega_i^r\right)^{\gamma(\dot{\varepsilon})}\frac{\partial\widetilde{W}^r\left(\lambda_i,\Omega_i^r;\dot{\varepsilon}\right)}{\partial \mathrm{X}_i}\ . \tag{B13}$$

By substituting this result into Eq. (B11) we obtain:

$$\lambda_i\frac{\partial\mathscr{W}^r}{\partial\lambda_i}=\Omega^r\lambda_i\left(\Omega_i^r\right)^{\gamma(\dot{\varepsilon})}\frac{\partial\widetilde{W}^r}{\partial \mathrm{X}_i}=\Omega^r \mathrm{X}_i\frac{\partial\widetilde{W}^r}{\partial \mathrm{X}_i}. \tag{B14}$$

which renders Eq. (28). Note that for simplicity we have dropped the notational dependence of $\widetilde{W}^r$ on $(\lambda_i,\Omega_i^r;\dot{\varepsilon})$.

References

Amin, A.F.M.S., Lion, A., Sekita, S., Okui, Y., 2006. Nonlinear dependence of viscosity in modeling the rate-dependent response of natural and high damping rubbers in compression and shear: experimental identification and numerical verification. Int. J. Plast. 22, 1610–1657. https://doi.org/10.1016/j.ijplas.2005.09.005.

Anssari-Benam, A., 2023a. Large isotropic elastic deformations: on a *comprehensive* model to correlate the theory and experiments for incompressible rubber-like materials. J. Elast. 153, 219–244. https://doi.org/10.1007/s10659-022-09982-5.

Anssari-Benam, A., 2023b. Comparative modelling results between a separable and a non-separable form of principal stretches–based strain energy functions for a variety of isotropic incompressible soft solids: ogden model compared with a parent model. Mech. Soft Mater. https://doi.org/10.1007/s42558-023-00050-z.

Anssari-Benam, A., Akbari, R., Dargazany, R., 2023a. Extending the theory of pseudo-elasticity to capture the permanent set and the induced anisotropy in the Mullins effect. Int. J. Non-Linear Mech. *under review*.

Anssari-Benam, A., Bucchi, A., 2018. Modelling the deformation of the elastin network in the aortic valve. J. Biomech. Eng. 140, 011004 https://doi.org/10.1115/1.4037916.

Anssari-Benam, A., Bucchi, A., 2021. A generalised neo-Hookean strain energy function for application to the finite deformation of elastomers. Int. J. Non-Linear Mech. 128, 103626 https://doi.org/10.1016/j.ijnonlinmec.2020.103626.

Anssari-Benam, A., Bucchi, A., Saccomandi, G., 2021. On the central role of the invariant I_2 in nonlinear elasticity. Int. J. Eng. Sci. 163, 103486 https://doi.org/10.1016/j.ijengsci.2021.103486.

Anssari-Benam, A., Bucchi, A., Screen, H.R.C., Evans, S.L., 2017. A transverse isotropic viscoelastic constitutive model for aortic valve tissue. R. Soc. Open Sci. 4, 160585 https://doi.org/10.1098/rsos.160585.

Anssari-Benam, A., Destrade, M., Saccomandi, G., 2022a. Modelling brain tissue elasticity with the Ogden model and an alternative family of constitutive models. Phil. Trans. R. Soc. A 380, 20210325. https://doi.org/10.1098/rsta.2021.0325.

Anssari-Benam, A., Horgan, C.O., 2022. A three-parameter structurally motivated robust constitutive model for isotropic incompressible unfilled and filled rubber-like materials. Eur. J. Mech. A Solids 95, 104605. https://doi.org/10.1016/j.euromechsol.2022.104605.

Anssari-Benam, A., Tseng, Y.-T., Bucchi, A., 2018. A transverse isotropic constitutive model for the aortic valve tissue incorporating rate-dependency and fibre dispersion: application to biaxial deformation. J. Mech. Behav. Biomed. Mater. 85, 80–93. https://doi.org/10.1016/j.jmbbm.2018.05.035.

Anssari-Benam, A., Tseng, Y.-T., Pani, M., Bucchi, A., 2022b. Modelling the rate-dependency of the mechanical behaviour of the aortic heart valve: an experimentally guided theoretical framework. J. Mech. Behav. Biomed. Mater. 134, 105341 https://doi.org/10.1016/j.jmbbm.2022.105341.

Anssari-Benam, A., Tseng, Y.-T., Pani, M., Bucchi, A., 2023b. A new dissipation function to model the rate-dependent mechanical behaviour of semilunar valve leaflets. J. Biomech. Eng. 145, 071004 https://doi.org/10.1115/1.4056917.

Bahrololoumi, A., Morovati, V., Shaafaey, M., Dargazany, R., 2021. A multi-physics approach on modeling of hygrothermal aging and its effects on constitutive behavior of cross-linked polymers. J. Mech. Phys. Solids 156, 104614. https://doi.org/10.1016/j.jmps.2021.104614.

Bergström, J.S., Boyce, M.C., 1998. Constitutive modeling of the large strain time-dependent behavior of elastomers. J. Mech. Phys. Solids 46, 931–954. https://doi.org/10.1016/S0022-5096(97)00075-6.

Dal, H., Gültekin, O., Açıkgöz, K., 2020. An extended eight-chain model for hyperelastic and finite viscoelastic response of rubberlike materials: theory, experiments and numerical aspects. J. Mech. Phys. Solids 145, 104159. https://doi.org/10.1016/j.jmps.2020.104159.

Dal, H., Açıkgöz, K., Badienia, Y., 2021. On the performance of isotropic hyperelastic constitutive models for rubber-like materials: a state of the art review. Appl. Mech. Rev. 73, 020802 https://doi.org/10.1115/1.4050978.

Dargazany, R., Itskov, M., 2009. A network evolution model for the anisotropic Mullins effect in carbon black filled rubbers. Int. J. Solids Struct. 46, 2967–2977. https://doi.org/10.1016/j.ijsolstr.2009.03.022.

Dargazany, R., Itskov, M., 2013. Constitutive modeling of the Mullins effect and cyclic stress softening in filled elastomers. Phys. Rev. E 88, 012602. https://doi.org/10.1103/PhysRevE.88.012602.

Doehring, T.C., Carew, E.O., Vesely, I., 2004. The effect of strain rate on the viscoelastic response of aortic valve tissue: a direct-fit approach. Ann. Biomed. Eng. 32, 223–232. https://doi.org/10.1023/B:ABME.0000012742.01261.b0.

Destrade, M., Saccomandi, G., Sgura, I., 2017. Methodical fitting for mathematical models of rubber-like materials. Proc. R. Soc. A 473, 20160811. https://doi.org/10.1098/rspa.2016.0811.

Garcia-Gonzalez, D., Rusinek, A., Jankowiak, T., Arias, A., 2015. Mechanical impact behavior of polyether–ether–ketone (PEEK). Compos. Struct. 124, 88–99. https://doi.org/10.1016/j.compstruct.2014.12.061.

Garcia-Gonzalez, D., Zaera, D., Arias, A., 2017. A hyperelastic-thermoviscoplastic constitutive model for semi-crystalline polymers: application to PEEK under dynamic loading conditions. Int. J. Plast. 88, 27–52. https://doi.org/10.1016/j.ijplas.2016.09.011.

Gent, A.N., 1996. A new constitutive relation for rubber. Rubber Chem. Technol. 69, 59–61. https://doi.org/10.5254/1.3538357.

Harwood, J.A.C., Mullins, L., Payne, A.R., 1965. Stress softening in natural rubber vulcanizates. Part II: stress softening effects in pure gum and filler loaded rubbers. J. Appl. Polym. Sci. 9, 3011–3021. https://doi.org/10.1002/app.1965.070090907.

Holzapfel, G.A., Simo, J.C., 1996. A new viscoelastic constitutive model for continuous media at finite thermomechanical changes. Int. J. Solids Struct. 33, 3019–3034. https://doi.org/10.1016/0020-7683(95)00263-4.

Hossain, M., Liao, Z., 2020. An additively manufactured silicone polymer: thermo-viscoelastic experimental study and computational modelling. Addit. Manuf. 35, 101395 https://doi.org/10.1016/j.addma.2020.101395.

Hossain, M., Navaratne, R., Perić, D., 2020. 3D printed elastomeric polyurethane: viscoelastic experimental characterizations and constitutive modelling with nonlinear viscosity functions. Int. J. Non-Linear Mech. 126, 103546 https://doi.org/10.1016/j.ijnonlinmec.2020.103546.

Hossain, M., Possart, G., Steinmann, P., 2009a. A finite strain framework for the simulation of polymer curing. Part I: elasticity. Comput. Mech. 44, 621–630. https://doi.org/10.1007/s00466-009-0397-0.
Hossain, M., Possart, G., Steinmann, P., 2009b. A small-strain model to simulate the curing of thermosets. Comput. Mech. 43, 769–779. https://doi.org/10.1007/s00466-008-0344-5.
Hossain, M., Vu, D.K., Steinmann, P., 2012. Experimental study and numerical modelling of VHB 4910 polymer. Comput. Mater. Sci. 59, 65–74. https://doi.org/10.1016/j.commatsci.2012.02.027.
Hrapko, M., van Dommelen, J.A.W., Peters, G.W.M., Wismans, J.S.H.M., 2006. The mechanical behaviour of brain tissue: large strain response and constitutive modelling. Biorheology 43, 623–636.
Kadapa, C., Hossain, M., 2022. A linearized consistent mixed displacement-pressure formulation for hyperelasticity. Mech. Adv. Mater. Struct. 29, 267–284. https://doi.org/10.1080/15376494.2020.1762952.
Kumar, A., Lopez-Pamies, O., 2016. On the two-potential constitutive modeling of rubber viscoelastic materials. C. R. Mecanique 344, 102–112. https://doi.org/10.1016/j.crme.2015.11.004.
Lee, E.H., 1969. Elastic–plastic deformation at finite strains. J. Appl. Mech. 36, 1–6. https://doi.org/10.1115/1.3564580.
Li, Y., Tang, S., Kröger, M., Liu, W.K., 2016. Molecular simulation guided constitutive modeling on finite strain viscoelasticity of elastomers. J. Mech. Phys. Solids 88, 204–226. https://doi.org/10.1016/j.jmps.2015.12.007.
Liao, Z., Yao, X., Zhang, L., Hossain, M., Wang, J., Zang, S., 2019. Temperature and strain rate dependent large tensile deformation and tensile failure behavior of transparent polyurethane at intermediate strain rates. Int. J. Impact Eng. 129, 152–167. https://doi.org/10.1016/j.ijimpeng.2019.03.005.
Linder, C., Tkachuk, M., Miehe, C., 2011. A micromechanically motivated diffusion-based transient network model and its incorporation into finite rubber viscoelasticity. J. Mech. Phys. Solids 59, 2134–2156. https://doi.org/10.1016/j.jmps.2011.05.005.
Lion, A., Höfer, P., 2007. On the phenomenological representation of curing phenomena in continuum mechanics. Arch. Mech. 59, 59–89.
Lubliner, J., 1985. A model of rubber viscoelasticity. Mech. Res. Commun. 12, 93–99. https://doi.org/10.1016/0093-6413(85)90075-8.
Mao, Y., Lin, S., Zhao, X., Anand, L., 2017. A large deformation viscoelastic model for double-network hydrogels. J. Mech. Phys. Solids 100, 103–130. https://doi.org/10.1016/j.jmps.2016.12.011.
Maugin, G.A., 1995. Material forces: concepts and applications. Appl. Mech. Rev. 48, 213–245. https://doi.org/10.1115/1.3005101.
Miehe, C., Göktepe, S., 2005. A micro–macro approach to rubber-like materials. Part II: the micro-sphere model of finite rubber viscoelasticity. J. Mech. Phys. Solids 53, 2231–2258. https://doi.org/10.1016/j.jmps.2005.04.006.
Mohammadi, H., Dargazany, R., 2019. A micro-mechanical approach to model thermal induced aging in elastomers. Int. J. Plast. 118, 1–16. https://doi.org/10.1016/j.ijplas.2018.12.009.
Morovati, V., Bahrololoumi, A., Dargazany, R., 2021. Fatigue-induced stress-softening in cross-linked multi-network elastomers: effect of damage accumulation. Int. J. Plast. 142, 102993 https://doi.org/10.1016/j.ijplas.2021.102993.
Morovati, V., Dargazany, R., 2019. Micro-mechanical modeling of the stress softening in double-network hydrogels. Int. J. Solids Struct. 164, 1–11. https://doi.org/10.1016/j.ijsolstr.2019.01.002.
Mullins, L., 1947. Effect of stretching on the properties of rubber. J. Rubber Res. 16, 275–289. https://doi.org/10.5254/1.3546914.
Naumann, C., Ihlemann, J., 2015. On the thermodynamics of pseudo-elastic material models which reproduce the Mullins effect. Int. J. Solids Struct. 69-70, 360–369. https://doi.org/10.1016/j.ijsolstr.2015.05.014.
Ogden, R.W., 1972. Large deformation isotopic elasticity – on the correlation of theory and experiment for incompressible rubberlike solids. Proc. R. Soc. Lond. A 326, 565–584. https://doi.org/10.1098/rspa.1972.0026.
Ogden, R.W., 2001. Pseudo-elasticity and stress softening. In: Fu, Y.B., Ogden, R.W. (Eds.), Nonlinear Elasticity: Theory and Applications. Cambridge University Press. https://doi.org/10.1017/CBO9780511526466.014.
Ogden, R.W., Roxburgh, D.G., 1999. A pseudo-elastic model for the Mullins effect in filled rubber. Proc. R. Soc. Lond. A 455, 2861–2877. https://doi.org/10.1098/rspa.1999.0431.
Ogden, R.W., Saccomandi, G., Sgura, I., 2004. Fitting hyperelastic models to experimental data. Comput. Mech. 34, 484–502. https://doi.org/10.1007/s00466-004-0593-y.
Pioletti, D.P., Rakotomanana, L.R., Benvenuti, J.-F., Leyvraz, P.F., 1998. Viscoelastic constitutive law in large deformations: application to human knee ligaments and tendons. J. Biomech. 31, 753–757. https://doi.org/10.1016/S0021-9290(98)00077-3.
Rajagopal, K.R., Srinivasa, A.R., 2004. On the thermomechanics of materials that have multiple natural configurations Part I: viscoelasticity and classical plasticity. Z. Angew. Math. Phys. 55, 861–893. https://doi.org/10.1007/s00033-004-4019-6.
Reese, S., Govindjee, S., 1998. A theory of finite viscoelasticity and numerical aspects. Int. J. Solids Struct. 35, 3455–3482. https://doi.org/10.1016/S0020-7683(97)00217-5.
Ricker, A., Gierig, M., Wriggers, P., 2023. Multiplicative, non-Newtonian viscoelasticity models for rubber materials and brain tissues: numerical treatment and comparative studies. Arch. Comput. Methods Eng. https://doi.org/10.1007/s11831-023-09889-x.
Ricker, A., Wriggers, P., 2023. Systematic fitting and comparison of hyperelastic continuum models for elastomers. Arch. Comput. Methods Eng. 30, 2257–2288. https://doi.org/10.1007/s11831-022-09865-x.
Rivlin, R.S., 1948. Large elastic deformations of isotropic materials IV. Further developments of the general theory. Philos. Trans. R. Soc. Lond. A 241, 379–397. https://doi.org/10.1098/rsta.1948.0024.
Simo, J.C., 1987. On a fully three-dimensional finite-strain viscoelastic damage model: formulation and computational aspects. Comput. Methods Appl. Mech. Eng. 60, 153–173. https://doi.org/10.1016/0045-7825(87)90107-1.
Srikanth, K., Sreejith, P., Arvind, K., Kannan, K., Pandey, M., 2023. An efficient mode-of-deformation dependent rate-type constitutive relation for multi-modal cyclic loading of elastomers. Int. J. Plast. 163, 103517 https://doi.org/10.1016/j.ijplas.2023.103517.
Steinmann, P., Hossain, M., Possart, G., 2012. Hyperelastic models for rubber-like materials: consistent tangent operators and suitability for Treloar's data. Arch. Appl. Mech. 82, 1183–1217. https://doi.org/10.1007/s00419-012-0610-z.
Treloar, L.R.G., 1943. The elasticity of a network of long-chain molecules - II. Trans. Faraday Soc. 39, 241–246. https://doi.org/10.1039/TF9433900241.
Wang, S., Chester, S.A., 2018. Experimental characterization and continuum modeling of inelasticity in filled rubber-like materials. Int. J. Solids Struct. 136-137, 125–136. https://doi.org/10.1016/j.ijsolstr.2017.12.010.
Xiang, Y., Zhong, D., Rudykh, S., Zhou, H., Qu, S., Yang, W., 2020. A review of physically based and thermodynamically based constitutive models for soft materials. J. Appl. Mech. 87, 110801 https://doi.org/10.1115/1.4047776.
Zhan, L., Wang, S., Qu, S., Steinmann, P., Xiao, R., 2023. A new micro–macro transition for hyperelastic materials. J. Mech. Phys. Solids 171, 105156. https://doi.org/10.1016/j.jmps.2022.105156.
Zhou, J., Jiang, L., Khayat, R.E., 2018. A micro–macro constitutive model for finite-deformation viscoelasticity of elastomers with nonlinear viscosity. J. Mech. Phys. Solids 110, 137–154. https://doi.org/10.1016/j.jmps.2017.09.016.